Development of an Experimental Model to Quantify Lumbar Spine Kinematics during Military Seat Ejection

Steven George Storvik
Marquette University

DEVELOPMENT OF AN EXPERIMENTAL MODEL TO QUANTIFY LUMBAR SPINE KINEMATICS DURING MILITARY SEAT EJECTION

by

Steven G. Storvik

A Thesis submitted to the Faculty of the Graduate School,
Marquette University,
in Partial Fulfillment of the Requirements for
the Degree of Master of Science

Milwaukee, Wisconsin

August 2011

ABSTRACT
DEVELOPMENT OF AN EXPERIMENTAL MODEL TO QUANTIFY LUMBAR SPINE KINEMATICS DURING MILITARY SEAT EJECTION

Steven G. Storvik

Marquette University, 2011

The initial phase of a military ejection sequence exerts substantial axial loads on the spinal column. Eccentric inertial loading on the thoracolumbar spine can lead to injury. Most serious injuries due to ejection are in the form of a vertebral fracture, most commonly occurring at the thoracolumbar junction. The objective of the current study was to understand characteristics of a military seat ejection by employing an experimental model designed to simulate the *boost or in-rail* phase. The model incorporates realistic boundary conditions and is capable of quantifying metrics associated with injury tolerance such as applied accelerations and resultant loads and spinal kinematics.

A total of four human cadaveric spine specimens (T12-L5) were tested. The test matrix consisted of two parts. The first part subjected specimens to sub-failure loading to outline spinal kinematics during dynamic vertical acceleration. The second part of the test matrix consisted of acceleration tests designed to induce compression and/or burst fractures as sustained by military aviators during ejection. The developed experimental model is the first to simulate realistic inertial loading during ejection-type accelerations using isolated osteoligamentous spines and may provide imperative injury mechanism data for future safety design considerations.

ACKNOWLEDGMENTS

Steven G. Storvik

First and foremost, I would like to thank and acknowledge my Lord and Savior, Jesus Christ. Amen.

Next, I thank my advisor Brian D Stemper, PhD. Dr. Stemper brought the initial vision for this research project to me, and has been patient and understanding throughout its progress. I sincerely appreciate the opportunities he has provided me, one of which was joining the Department of Neurosurgery at the Medical College of Wisconsin. It has been a humbling honor and privilege to work in the same lab as Frank A. Pintar, PhD and Narayan Yoganandan, PhD.

I would like to thank Gerald F Harris, PhD and Jamie L Baisden, MD for completing an incredible list of committee members. Their vast expertise has added strength to this completed work. I would also like to acknowledge Barry S. Shender, PhD and Glenn R. Paskoff for providing technical guidance throughout the development of this new experimental model.

I am thankful for Michael Schlick, Christy Stadig, Kristen Reichart, Paul Gromowski, Steve Tilistyak, and Alok Shah. Their positive attitudes, laughs, and assistance in day-to-day research activities have made my graduate career successful and memorable.

Finally, I have been blessed to be someone loved. I owe a deep debt of gratitude to my parents, Steven and Gail Storvik, and to my wife, Aneta, for providing support and guidance.

This research was supported in part by the Office of Naval Research through Naval Air Warfare Center Aircraft Division Contract N00421-10-C-0049 and the Department of Veterans Affairs Medical Research.

TABLE OF CONTENTS

LIST OF TABLES

LIST OF FIGURES

CHAPTER 1: BACKGROUND

1.1 Justification for Research

Military ejection seats exert substantial axial loads on the spinal column during the *boost or in-rail* phase as the seat must vertically displace the aviator over a very short time period [1]. A serious resulting injury of particular concern is spinal injury in the form of vertebral fractures. Clinical studies investigating the relative frequency of vertebral fractures after ejection have reported rates of 16 to 38% [2-8]. These fractures most commonly affect the thoracolumbar junction [2,9,10]. Recent ejection data, lumping aircraft and performance envelope types, indicate that between 20 and 60% of vertebral fractures sustained by survived ejectees occur between the twelfth thoracic vertebra (T12) and the fifth lumbar vertebra (L5) [6-8]. Therefore, an improved understanding of the dynamic response of the lumbar spine during axial loading is required to advance aviator safety during seat ejection.

Isolated post-mortem human subject (PMHS) or bovine/porcine spines have been utilized in the past to investigate lumbar mechanics. The method of load application most often involved static specimen placement with dynamic load application to the superior fixation using weight-drop [11-17] or MTS piston [18-24] techniques. Often these experimental models were used to make available clinically relevant data concerning vertebral fractures, such as compressive failure thresholds, canal encroachment data, and comparisons of reduction techniques. However, experimental boundary conditions affect the mechanism of injury and, thus, should accurately simulate

the real-world loading scenario in order to obtain accurate and applicable data. For example, Ewing et al. stated that ejection fractures "are not due to blunt trauma to the vertebrae, nor to striking the aircraft or ground, but appear to occur during or slightly subsequent to initial application of vertical $+G_Z$ impact [acceleration] to the vertebral column" [25]. Therefore, inertial loading of the upper torso may have a considerable role in injury causation and is an important boundary condition to incorporate. Furthermore, the MTS piston and the weight-drop models in their current forms are not practical to investigate input $+G_Z$ acceleration that can be directly related to the *boost or in-rail* phase of a military seat ejection. In other words, characteristics of the caudocephalad acceleration pulse applied to the seat during ejection can not be explicitly related to the presence/absence or type of vertebral fracture produced during an experimental test using these models. What's more, characteristics of the acceleration versus time pulse, such as maximum acceleration, duration, and rate of onset, are important in producing clinically-relevant injury types and severities [12], and has not been thoroughly investigated using these two previous models. An investigation of acceleration input will have direct application to develop safer ejection seats.

To fully understand injury mechanisms and characteristics of the lumbar spine during a military seat ejection, an archetypal axial loading scenario, a biomechanically accurate and repeatable model capable of fully quantifying metrics associated with injury tolerance (i.e., accelerations, loads, kinematics) must be used. Thus, the current study focused on the development of an experimental model that would accurately quantify the biofidelic response of PMHS thoracolumbar spines during dynamic axial loading using realistic boundary conditions. Understanding the specific mechanism of injury is the first

step in developing strategies for injury prevention. Accordingly, delineating the effects of these factors is imperative for future safety design considerations not only for ejection seats, but also for other like axial loading scenarios such as falls from height, military underbody blast due to improvised explosive devices, and motor vehicle bottoming out.

1.2 Thoracolumbar Spine Biomechanics

1.2.1 Anatomical Consideration

Subject to traumatic axial loading, the spine most often experiences serious injuries at the thoracolumbar junction [26-29]. The thoracolumbar junction (T11-L2) is unique anatomically and consequently biomechanically. An understanding of the structural geometry may help explain in part the higher frequency of injury at this site.

The spinal column consists of four regions (cervical, thoracic, lumbar, sacral) and two curvatures. The cervical and lumbar regions have a lordotic curvature and the thoracic and sacral regions have a kyphotic curvature. At the thoracolumbar junction, the spinal column is transitioning inferiorly from kyphosis to lordosis. Also a point of interest, the facet orientation is at a transitioning point and the floating ribs begin at the junction. Combining these facts can pose possible reasons why this site is prone to axially induced injuries on the spinal column.

Kyphosis in the thoracic spine usually begins at T1-T2, averaging about 1^{o} at that segment [30]. The kyphotic angulation incrementally increases at each segment caudally until the apex of the kyphosis at T6-T7. From T4-T5 to T8-T9, roughly 5^{o} of kyphosis

occurs at each segment. The kyphosis incrementally decreases below the apex until the thoracolumbar junction, where the normal segmental angulation at T11-T12, T12-L1, and L1-L2 is 2.5^{o} kyphosis, 1^{o} kyphosis, and 4^{o} lordosis, respectively [30]. Lumbar lordosis begins at L1-L2 and incrementally increases caudally to the sacrum. The lumbar lordosis apex occurs at the L3-L4 disc. Thus, the thoracolumbar junction is a transitioning point from lordosis to kyphosis and acts as a fulcrum between the thorax and lower back.

In the transverse plane, the facet angles are an average of 106^{o} from T1 to T11 (T10 in the inferior facets), defining the transverse angles as the angle between the lines of the mid-sagittal plane and the articular facet widths of each vertebra [31]. From T12 to L2 (from T11 to L2 in the inferior facets) the facet angles rapidly decrease sequentially with L2 having a mean of 25^{o} (Fig. 1). Then, from L3 to L5 the facet angles increase steadily reaching an average of 50^{o}. In the sagittal plane, the facet angles are at a transitioning point in a similar manner at the thoracolumbar junction location. Whereas the facet angles are generally frontally oriented in the cervical region and manifest a slight anterior inclination from the frontal plane in the thoracic region, the facets are dramatically sagittaly oriented in the lumbar. This results in the lumbar spine having minimal resistance to flexion compared to the thoracic spine, and therefore a larger flexion-extension range of motion (ROM) [32]. In the upper and middle thoracic regions the ROM is 4 and 6 degrees, respectively. At T11 through L2, however, the ROM is increased to 12 degrees [33].

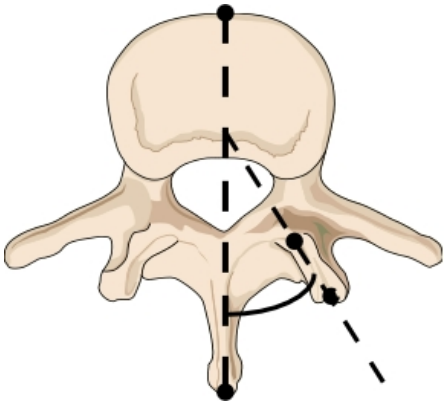

Figure 1: Illustration describing facet angle definitions in the transverse plane.

Another key component to consider is the rib cage. The rib cage increases the thoracic spine's moment of inertia and, therefore, its stiffness and strength in any mode of bending. In axial compression, the rib cage and sternum provide 21% of the stiffness [34]. In flexion-extension, it was shown that 40% of the thoracic spine stiffness was provided by the rib cage and sternum. In another biomechanical investigation of the thoracic spine, resection of the costovertebral joints after discectomy increased ROM by approximately 80% under all loading modes. While the costovertebral joints are attached to two vertebral bodies from T1 to T10, the ribs are entirely attached to the body on T11 and T12. T11 and T12 lack a costotransverse articulation as well. Thus, the added stability and shared load path is lost at this region. Although the ribcage increases the thoracic spine's strength and stiffness in bending, it moves the center of gravity of the torso further anterior from the instantaneous axis of rotation of inferior motion segments. Consequently, a larger flexion moment is produced and the region just caudal to T10 becomes most susceptible to injury during axial loading.

During axial loading, therefore, the upper and middle thoracic spine has a tendency to resist flexion and transfer its inertial load first compressively to the

thoracolumbar junction. At this site, the stability gained by the rib cage is lost, and the spine becomes less resistant to flexion due to the increasingly sagittally oriented facet joints. What's more, the posterior ligamentous complex and musculature organization of the lumbar spine is apt to maintain lordosis, and may attempt to keep its cranial end upright during a dynamic event. While the vertebrae of the thoracolumbar junction have lumbar characteristics, relatively, they are less strong than L3-L5 in axial loading [35]. Theoretically, this setting will leave T11-L2 predisposed to anterior wedge fractures. Clinical literature supports this assertion by identifying that (anterior wedge) compression fractures are the most common injury to occur at this location along the spinal column [29,36,37].

1.2.2 Compression/Compression-Flexion Failure

Kazarian and Graves made an outstanding contribution to experimental spinal biomechanics in 1977. Using isolated human thoracic vertebral bodies (age: 31 ± 6 years), the biomechanical investigation highlighted uniaxial compressive strength characteristics related to strain rate and position along the spinal column. Considering ultimate load and stiffness of the centrum, the effects of position and displacement rate were statistically significant [38]. The study revealed that ultimate load and stiffness increased with descending position along the spinal column and with increasing displacement rate. At a quasi-static loading rate of 0.0889 mm/s the average ultimate load was 3898 ± 1288 N (n = 16). At an increased loading rate of 889 mm/s the average ultimate load increased to 8692 ± 3329 N (n = 29). The axial deformation to ultimate

load, however, is only dependent on rate and not on position – the higher the loading rate, the lower the deformation of the body at ultimate load. When simultaneous anterior bending is included, the compressive failure load is reduced [39]. Isolated T9 or T10 centrums loaded at 0.1 mm/s axial displacement and 0.2 ^{o}/s anterior rotation failed at an average of 1750 ± 898 N compressive force and 27 ± 19 Nm flexion moment. Thus, the mechanical behavior of vertebral bodies in compression varied with loading conditions.

In comparison to thoracic vertebrae, compressive strength of individual lumbar vertebrae has also been investigated. Pure compression tests of one-vertebra lumbar specimens, including 3 mm of disc on each endplate, were conducted at a quasi-static displacement rate of 0.0833 mm/s [35]. For male specimens (n = 45; age: 60 ± 15 years), average ultimate load for L1-L4 was 4570 ± 2137 N. Eight younger specimens, similar in age to the specimens from the Kazarian and Graves study, however, had an average ultimate load of 7351 ± 2711 N. Therefore, compressive strength of lumbar vertebrae is an average of 89% greater than thoracic vertebrae.

It is well accepted that vertebral centrum strength increases descending the spinal column and that the failure load is correlated to bone quality [38,40-42]. The mean increase in failure load between T10 and L5 is 0.24 kN per segment. Although using the single segment approach provides a more specific assessment of the strength and mechanical behavior of an individual vertebra, testing functional units and multi-segment specimens more accurately simulates in vivo loading conditions. The interaction among the vertebral bodies, intervertebral joints, and ligaments largely affect the spine's mechanical response to loading and present multiple modes of failure (e.g., vertebral

body failure, endplate fracture, prolapsed disc). Accordingly, a majority of past biomechanical investigations have tested single or multiple functional units in series.

Yoganandan et al. investigated normal and degenerated functional units in pure compression at a quasi-static rate of 2.54 mm/s [43]. Degenerated specimens had lower average failure loads (5.30 ± 0.29 kN) than normal specimens (11.03 ± 1.42 kN). The study showed that strain energy absorption capacity is significantly higher for normal compared to degenerated specimens, although, the deflections were approximately the same. Another study, conducted by Hutton and Adams, reported similar compression strength when applying compression to functional units pre-flexed 4 to 10 degrees, and revealed that endplate fracture was the mode of failure in 85% of the cases [44]. Although the group did not report the inherent flexion moment with the concomitant compression force, Adams et al. reported the typical failure flexion moment to be between 49 and 73 Nm [45,46]. Whereas single-vertebra testing characterized trabecular and cortical bone strength of the vertebra, testing functional units provided evidence that the soft tissue organization and the composite nature of the spine affect load sharing and injury mechanism. For a concise summary of past experimental investigations of functional units in compression, refer to [43].

During compressive loading of the vertebra, the tissue near and including the endplates is at the highest risk of initial failure [47]. Consequently, several studies have focused on characterizing the endplate's role in injury mechanism. Much like vertebral bodies, superior and inferior lumbar endplates' failure loads increase from L1 to L5 [48]. The biomechanical load-deformation response of lumbar endplates has been investigated by compressing the entire vertebra-disc interface and also by using a hemispherical

indenter to perform indentation tests at various sites directly on the endplate surface. The two test setups produce fundamentally different boundary conditions. Local deformations were recorded as high as 1.5 mm under 110 N compression using indentation tests [48]. These tests revealed that the posterolateral regions of lumbar endplates are the strongest. However, when 2-vertebra specimens were compressed, and the disc proportionally loaded the endplate, maximum displacements of 0.4 mm under 5.5 kN compressive force were recorded [49]. Fractured or permanently bulged endplates were obtained from an average of 3075 ± 435 N compressive force [49].

Not only do the specimen boundary conditions affect resulting injuries, but so does the rate of external loading. In 1997, Yingling et al. loaded to failure three-vertebra porcine spines at five loading rates ranging from 100 to 16000 N/s. A significant effect of load rate on the ultimate compressive load, displacement, and stiffness at failure resulted from the three-way multivariate analysis of variance, supporting the earlier study by Kazarian and Graves. What's more, the study revealed that as loading rate changes from quasi-static to dynamic, the failure site shifts from exclusively endplate to vertebral body failures. Thus, the decrease in deformation at failure as loading rate increases together with the shifting of injury from the endplate to the vertebral body suggest a change in the injury mechanism between quasi-static and dynamic loading [50].

Extensive research has been conducted using isolated osteoligamentous spine specimens to investigate resulting injuries due to compression/compression-flexion loading. These studies have provided a wide range of load-tolerance values for compression and flexion, the primary spinal motions resulting from ejection [10]. To focus the literature search toward fracture patterns observed in survived ejectees [37],

relevant experimental studies investigating the anterior wedge fracture and more severe burst fracture are discussed in the following section.

1.3 Prior Vertebral Fracture Models

Numerous researchers have sought to characterize spinal fractures due to dynamic vertical loading. Most often, the specific aims were to clarify the mechanism, observe the fracture pattern, measure the spinal canal occlusion, compare surgical or conservative management outcomes, or examine the general mechanical behavior of the injury. In order to achieve these aims, two vertebral fracture models have been incorporated in a majority of studies – the weight-drop model and the MTS piston model (Fig. 2). These models involve fixing the caudal end of the specimen and applying a vertical load to the cranial end. From these past studies, several important design considerations can be derived that are pertinent to the development of an experimental model. However, scrutiny of these studies also reveals that existing models are inadequate to characterize the thoracolumbar spine during military seat ejection.

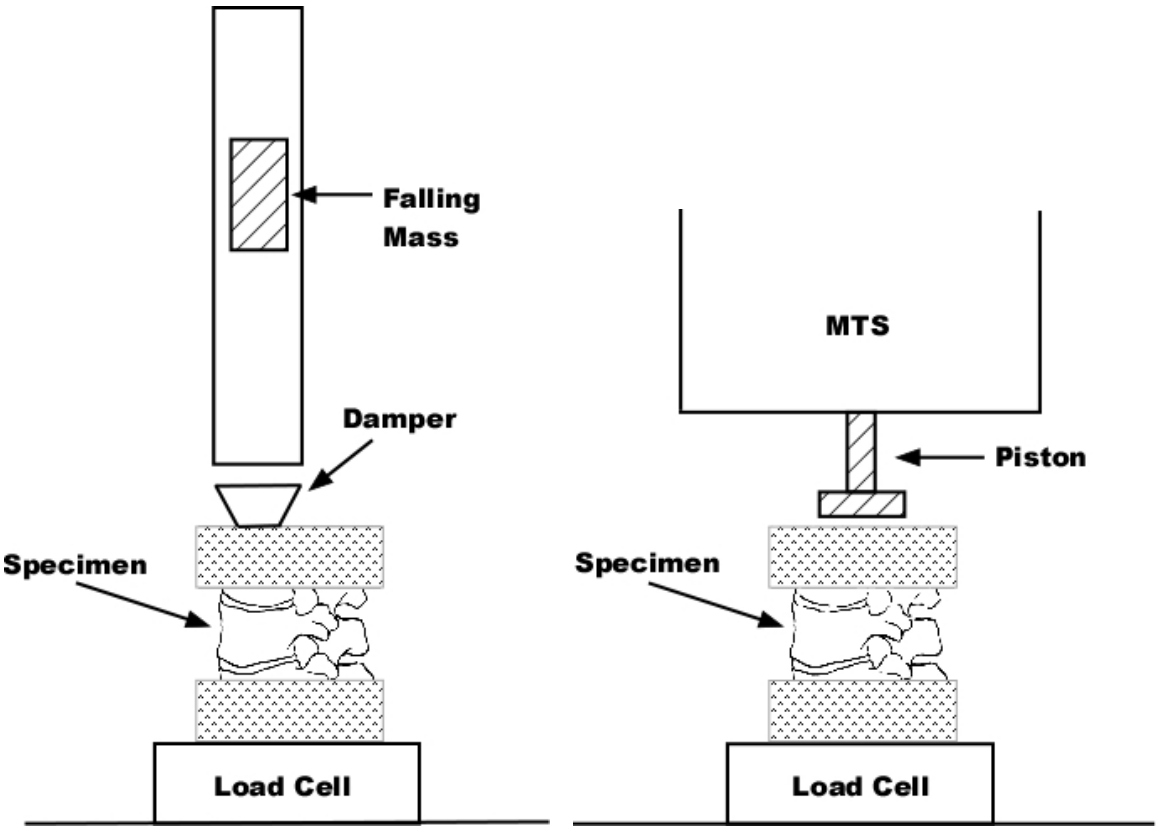

Figure 2: Representative drop-weight model (left) and MTS model (right).

The initial phase of an ejection sequence, the *boost or in-rail* phase, is a dynamic event. Previously reported seat acceleration data suggest that operational peak and onset rates range between 14 – 21 g and 175 – 300 g/s, respectively [51-53]. Simulated ejections at presumed sub-injury acceleration levels using USAF-fit volunteers showed that the average compressive loading rate measured on the seat pan due to 10 g peak accelerations (8 m/s) reached in approximately 70 ms was 150 kN/s [54]. Since the spine is a viscoelastic structure, it's response to external loading is rate dependent. Accordingly, loading rate is an important aspect to consider.

Early researchers studying spinal biomechanics acknowledged the importance of loading rate. To dynamically load the spine a mass was dropped from a height onto the cranial end. This method was first described by Hirsch and Nachemson in 1954 [55]. A widely referenced work by Perey in 1957 reported injury types in functional units using the drop-weight method [56]. These experiments produced maximum loads between 10,300 and 13,200 N within 6 ms by dropping a mass of 15 kg from a height of 0.5 meters. This corresponds to a potential energy (PE) of 74 joules. Endplate fractures occurred in 26% of the experiments; wedge-shaped vertebral compression fractures occurred in 8%. Willen et al. produced more severe compression (burst) fractures by dropping 10 kg masses from 2 meters (PE = 196 J) onto three-vertebra thoracolumbar specimens [13]. The group noted that vertebrae from subjects above seventy years of age tended to collapse totally in compression due to dynamic axial loading, whereas vertebrae from subjects under forty years of age showed the comminuted fracture pattern characteristic of burst fractures [29]. These experimental data agreed well with clinical data wherein patients sustaining burst fractures were typically young [57,58]. Subsequent studies provided supporting results, confirming that the burst fracture was a high rate injury (Table 1).

These data, however, were derived from two- or three-vertebra specimens and cannot be used to directly deduce the response of the entire lumbar spine. In functional unit testing, free motion in the facet joints was not allowed [59]. In three-vertebra segments, consisting of three vertebrae and the two intervening intervertebral discs, free motion was allowed and in vivo loading was better simulated on both the proximal and distal ends of the vertebra of interest. However, only one vertebra was exposed to

traumatic loading and longitudinal ligaments spanning several vertebrae are transected in this setup. Again, the response of the entire lumbar spine was restricted, and the response data from these studies are less bona fide to directly validate a full, intact lumbar spine FE model.

Specimen lengths greater than three vertebrae were not biomechanically tested until the late 1980's. Yoganandan et al. tested full lumbar spine columns at a quasistatic rate of 2.5 mm/s under the compression-flexion mode until failure using the MTS piston model. Initial failure of the column occurred at an average load of 3815 ± 473 N [22]. In a later study, Duma et al. tested full lumbar spine columns at a dynamic rate of 1000 mm/s [18]. Those spines failed at an average compression force of 5460 ± 638 N and flexion moment of 201 ± 51 Nm ([22] did not report concurrent flexion data). Although the two data sets cannot be directly compared since the fractures were biased by stress risers in the study by Yoganandan et al., it is worth noting that the spines under high-rate loading exhibited a 40% increase in ultimate load. This characteristic trend is supported by an earlier study wherein intact spines failed at an average compression force of 2329 ± 1515 N and flexion moment of 167 ± 75 Nm under quasistatic compression-flexion [60]. However, these values are only presented for comparison as those spines were much longer in length. Over 70% of specimens tested were T2- or T3-L5.

Dynamic studies of the isolated osteoligamentous spine using the drop-weight method are listed in Table 1; dynamic studies using the MTS method are listed in Table 2. Although these models have provided clinically relevant data concerning the fractures produced, such as canal encroachment data and comparisons of reduction techniques, the models have not fully characterized the injury mechanism. In general, the majority of

studies have defined tolerance thresholds in terms of forces and moments, albeit without scenario-specific boundary conditions. For example, two boundary conditions that have not been given the attention they deserve are realistic inertial loading and the input acceleration pulse. The caudal end of the specimen was always rigidly fixed in the global coordinate system, giving this end of the specimen a constant acceleration of zero. While this boundary condition is experimentally expedient, it does not replicate the inertial loading present during real-world axial loading situations such as military pilot ejection. In addition, characteristics of the acceleration versus time pulse, such as maximum acceleration, duration, and rate of onset, are important in producing clinically-relevant injury types and severities, and defining injury tolerance thresholds [12]. Past studies using both the MTS piston model and weight-drop model have not thoroughly examined these two areas of focus.

Weight-drop or piston load application to the cranial fixation does not replicate the acceleration-driven loading as applied to the base of the spine in pilot ejection, as well as many other real-world axial loading scenarios. Depending upon the rate of onset of acceleration during the *boost or in-rail* phase, motion of the upper torso supported by the spine may lag the forced motion of the seat pan with accompanying spinal compression [53]. At this point, under such conditions, the seat has a greater velocity than the upper torso, which subsequently requires the upper torso to undergo an acceleration which exceeds seat acceleration in order to reach terminal seat velocity. Early researchers in the mid-twentieth century referred to this phenomenon as the “dynamic response” [51,52,61,62]. This mechanical phenomenon is of considerable importance in injury causation, and was investigated initially using continuum models of the spine. It was

shown that the dynamic response is much more sensitive to changes of rate of acceleration onset than the final velocity. Hess et al. showed that for small rise times (< 40 ms) the maximum acceleration and stress that the spinal column experienced increased to twice the value of rise times over 100 ms [63]. Therefore, realistic inertial loading is important in characterizing military seat ejection.

Acceleration data were not widely reported in dynamic studies involving isolated osteoligamentous spines. The actual acceleration of the superior and inferior ends of the specimen has not been reported, though, the inferior end can be assumed to be zero for the duration of the test. Willen et al. recorded the acceleration history of the falling mass as it impacted the superior end of the specimen, reporting a maximum acceleration over 80 g within 10 ms of the event [13]. The loading paradigm lasted less than 15 ms. Other studies utilizing the drop-weight method had similar loading histories. The entire drop-weight event (loading and unloading) typically had a total duration between 20 and 30 ms, reaching peak compression loads within 10 ms [64,65]. Only one study reported a greater mean time to peak load [12]. This particular study used bovine spines, and reached peak compression loads within 20 ms.

Table 1: Dynamic PMHS thoracolumbar spine injury investigations utilizing weight-drop method.

First author	Year	Journal	Column length	Specimens tested	Failure compression (N)	Failure moment (Nm)	Object investigated	Initial Specimen Orientation	Specimen integrity intact	Comments
Perey	1957	Acta Orthop Scand Suppl	2-vertebra	Human; 9x T12-L1, 12x L1-L2, 21x L2-L3, 14x L3-L4, 20x L4-L5	Approximate range: 10,300 – 13,200	-	Injury mechanism & mechanical behavior	Neutral	Yes	Compression approximated using weight-drop method
Willen	1984	Spine	3-Vertebra	Human; 7x T12-L2	Range: 6,000 – 10,000	-	Injury mechanism & morphology, reduction effects	Neutral	Yes	Compression recorded at initial fracturing
					Range: 9,500 – 12,000	-				Compression recorded during further compression and consecutive fracturing
Cotterill	1987	J Orthop Res	> 3-Vertebra**	Bovine; 20x T1-L6	-	-	Develop burst fracture model, reduction effects	15 deg flexion	No	**Only disc T12-T13 and half of vertebra T12 was exposed to trauma loading
Fredrickson	1988	Spine	> 3-Vertebra**	Human; 4x T10-L4	-	-	Canal encroachment, reduction effects	Neutral	Yes	**Only the vertebral level of interest was exposed to trauma loading

Table 1. (contd.)

First Author	Year	Journal	Column Length	Specimens tested	Failure Compression (N)	Failure Moment (Nm)	Object investigated	Initial Specimen Orientation	Specimen integrity Intact	Comments
Fredrickson	1992	Spine	> 3-Vertebra**	Human; 6x T10-L4	-	-	Canal encroachment, injury morphology, reduction effects	Neutral	Yes	** Only L1 was exposed to trauma loading
Cain, Jr.	1993	Spine	> 3-Vertebra**	Bovine; 24x T8-L3			Develop burst fracture model, reduction effects	Unspecified degree of flexion applied to caudal segment	Yes	**Only T12 was exposed to trauma loading
Zou	1993	Spine	> 3-Vertebra**	Human; 6x T10-L4	-	-	Reduction effects	Neutral	Yes	** Only L1 was exposed to trauma loading
Lin	1993	Spine	3-Vertebra	Human; 8x T11-L1, 2x T12-L2	-	-	Reduction effects	Neutral	Yes	
Panjabi	1994	Spine	3-Vertebra	Human; 13x T11-L1	-	-	Injury instability	Neutral	Yes	
Oxland	1994	J Spinal Disord	3-Vertebra	Human; 11x T11-L1 and 2x T12-L2	-	-	Injury instability	Neutral	Yes	
Panjabi	1995	Spine	3-Vertebra	Human; 14x T11-L1 and 2x T12-L2	6,680 ± 2,014	44 ± 66	Injury instability	Neutral	Yes	
					6,187 ± 2,286	93 ± 56		15 deg flexion	Yes	
Kifune	1995	Eur Spine J	3-Vertebra	Human; 10x T11-L1	Range: 5,300 – 6,800	-	Injury morphology & instability	8 deg flexion	Yes	

Table 1. (contd.)

First Author	Year	Journal	Column Length	Specimens tested	Failure Compression (N)	Failure Moment (Nm)	Object investigated	Initial Specimen Orientation	Specimen integrity Intact	Comments
Panjabi	1995	J Spinal Disord	3-Vertebra	Human; 15x T11-L1	-	-	Canal encroachment	8 deg flexion	Yes	
Tran	1995	Spine	3-Vertebra	Bovine; 3x T9-T11, 3x T11-T13, 3x L1-L3, and 3x L4-L6	4,700 (typical)	-	Injury mechanism & morphology, reduction effects	Neutral	Yes	Compression recorded using weight-drop method
Kifune	1997	J Spinal Disord	3-Vertebra	Human; 19x T11-L1	-	-	Injury morphology, canal encroachment	8 deg flexion	Yes	
Mermelstein	1998	Spine	> 3-Vertebra	Human; 6x T10-L3	-	-	Reduction effects	10 deg flexion	No	A burst fracture was created with the weight-drop method
Panjabi	1998	Eur Spine J	3-Vertebra	Human; 10x T11-L1	6,600	-175 (extension)	Injury instability	8 deg flexion	Yes	Failure compression and moment is from one representative specimen.
Panjabi	2000	Clin Biomech	> 3-Vertebra**	Human; 9x T11-L3	-	-	Incremental trauma approach, canal encroachment	8 deg flexion	Yes	**Tight-fitting epoxy collars were around T12 and L2 to protect these vertebrae

Table 1. (contd.)

First Author	Year	Journal	Column Length	Specimens tested	Failure Compression (N)	Failure Moment (Nm)	Object investigated	Initial Specimen Orientation	Specimen integrity Intact	Comments
Panjabi	2001	Spine	> 3-Vertebra**	Human; 9x T11-L3	-	-	Reduction effects	8 deg flexion	Yes	**Tight-fitting epoxy collars were around T12 and L2 to protect these vertebrae
Wilcox	2003	J Bone Joint Surg Am	3-Vertebra	Bovine; Thoracolumbar segments (unspecified)	-	-	Canal encroachment	Neutral	Yes	
Atlas	2003	Eur Spine J	2-Vertebra	Porcine; 10x L2-L3, 10x L4-L5	-	-	Incremental trauma approach	Neutral	Yes	
Wang	2007	J Neurosurg Spine	3-Vertebra	Bovine; 20x T12-L2	-	-	Incremental trauma approach	Neutral	Yes	
Kallemeier	2008	J Spinal Disord Tech	> 3-Vertebra	Human; 9x T11-L3			Reduction effects	15 deg flexion	No	

Table 2: Dynamic PMHS thoracolumbar spine injury investigations utilizing MTS method.

First Author	Year	Journal	Column Length	Specimens tested	Loading Rate	Failure Compression Load (N)	Failure Moment Load (Nm)	Study Goal	Specimen orientation	Specimen integrity Intact	Comments
Shono	1994	Spine	> 3-Vertebra**	Human; 24x T10-L4	10% of its original height in 0.5 seconds	7,199 Range: 3,303 – 12,535	-	Develop burst fracture model, reduction effects	Neutral	Yes	**Only the L1 vertebra was exposed to trauma loading
Langrana	2002	Spine	3-Vertebra	Human; 2x T10-T12, T11-L1	100 mm/s	2,809 ± 744	-	Injury mechanism	Neutral	Yes	
				Human; 3x T12-L2		5,802 ± 1,759	-		15 deg extension	Yes	
				Human; 2x T8-T10, T10-T12		5,255 ± 365	-		Neutral	Yes	Posterior elements removed prior to testing
Ochia	2002	Spine	3-Vertebra	Human; 21x unspecified thoracolumbar segments	10 mm/s	3,323 ± 1,231	-	Injury mechanism	Neutral	Yes	
					2,500 mm/s	4,154 ± 1,737					

Table 2. (contd.)

First Author	Year	Journal	Column Length	Specimens tested	Loading Rate	Failure Compression Load (N)	Failure Moment Load (Nm)	Study Goal	Specimen orientation	Specimen integrity Intact	Comments
Ochia	2003	J Biomech	1-Vertebra	Human; 19x L4, 2x L5	10 mm/s	120 ± 57	-	Injury mechanism	Neutral	Yes	Endplate fracture
						4,909 ± 2,729	-				Vertebral body fracture
					2,500 mm/s	623 ± 271	-				Endplate fracture
						9,700 ± 2,111	-				Vertebral body fracture
Duma	2006	Biomed Sci Instrum	> 3-Vertebra	Human; 2x T12-L5	1,000 mm/s	5,009 and 5,911	237 and 165	Biomechanical response	Distal end of L5 was at an angle of 18 deg.	Yes	Both failures (compression fractures) occurred at T12
			2-Vertebra	Human; L1-L2, L2-L3, L3-L4, L4-L5	1,000 mm/s	12,411 ± 829	70 ± 19		Neutral	Yes	All tests resulted in endplate fractures

By inference of the literature, determination of injury mechanism should be based effectually on appropriate specimen and external loading boundary conditions. To characterize a seat ejection sequence, in particular, careful selection of boundary conditions will create realistic loading and the mechanism of injury can be more precisely examined.

First, the specimen length should be greater than three-vertebra. Full columns are more appropriate, and may be advantageous, because longitudinal ligaments spanning several vertebrae are uninterrupted and the curvature of the spine remains intact. Furthermore, the response data collected would be justifiable to validate a full, intact lumbar spine FE model. Secondly, external loading should consist of dynamic compression-flexion. Particularly during $+G_Z$ acceleration, the spinal column is subjected to anterior bending due to the eccentricity of the viscera and rib cage of the torso [66,67]. Applied acceleration to the caudal extent of the specimen should reach 14 to 21 g within 100 and 200 ms. The compressive loading rate should be on the order of magnitude of 150 kN/s [54]. Thirdly, testing should apply acceleration-driven loading to the caudal extent. Past injury models (Tables 1 and 2) involve fixing the caudal end of the specimen in the global coordinate system, preventing realistic inertial loading. The vertebral fractures sustained by ejectees are not due to blunt trauma to the vertebrae, but appear to occur during initial application of $+G_Z$ acceleration to the distal end of the vertebral column [25]. Thus, the most common compression fractures are due to inertial loading of the upper torso during the *boost or in-rail* phase. Simulating this mechanical phenomenon is a critical component to characterizing pilot ejection.

1.4 Objectives

The aim of the project was to develop an experimental model to quantify segmental kinematics in addition to overall kinematics and kinetics of the PMHS thoracolumbar spine during dynamic axial loading using realistic boundary conditions. The completed work will represent the most comprehensive response data of the thoracolumbar spine to date, and will include quantified metrics that have been incorporated in past established injury criteria (i.e., accelerations, loads, kinematics). These data can be directly used by safety engineers to develop safer military ejection seats and civilian environments. Furthermore, it is the first experimental investigation simulating realistic inertial loading with an isolated osteoligamentous spine under these types of axial accelerations. The developed experimental model may provide the most biomechanically accurate injury model for studying burst and compression fractures, allowing successful prediction of injury given a specific $+G_Z$ acceleration input. Additionally, the data obtained herein may be used to validate computational model of the entire, intact lumbar spine, initiating parametric studies investigating injury mitigation.

CHAPTER 2: MATERIALS AND METHODS

2.1 Experimental Setup

The experimental model was designed to mimic axial loading exerted on the lumbar spine during military seat ejection. The loading device consisted of two horizontal platforms attached to a vertical monorail [68]. The two decoupled platforms were connected to each other using a cable (Fig. 3). The cable connected the lower platform to the upper and allowed ease of positioning the initial vertical distance between platforms without preloading the specimen. The caudal end of the specimen was rigidly fixed to the lower platform through a six-axis load cell (Robert A. Denton Inc., Rochester, MI). The instantaneous center of rotation of T12 about the fixed sacrum in the sagittal plane follows the path traversed by the L3 vertebral body [69]. Accordingly, the specimen was mounted to the six-axis load cell so that the posterior longitudinal ligament (PLL) of L3 was aligned with the center of the force and moment axis system. This alignment provided the best approximation of measured loads as T12 bends in relation to the relatively immobilized base, L5. Uniaxial accelerometers (Endevco Corp., San Juan Capistrano, CA) were attached to upper and lower platforms to record vertical acceleration. Mass was added to the upper platform to simulate the weight of the head, neck, thorax, and upper extremities (refer to Section 2.4 for further details). The upper platform loaded the specimen superiorly via a laterally-oriented cylinder that extended across the entire superior PMMA casting. Friction was added to the interaction between the loading cylinder and the superior PMMA casting to prevent slippage by wrapping the

cylinder in gauze and placing compressed foam on the superior surface of the PMMA casting. The loading cylinder was mounted to the upper platform through a telescoping linkage to allow continuous range of positioning in the anteroposterior direction. This feature allowed the device to apply different flexion/extension moments while keeping the compression force approximately unchanged.

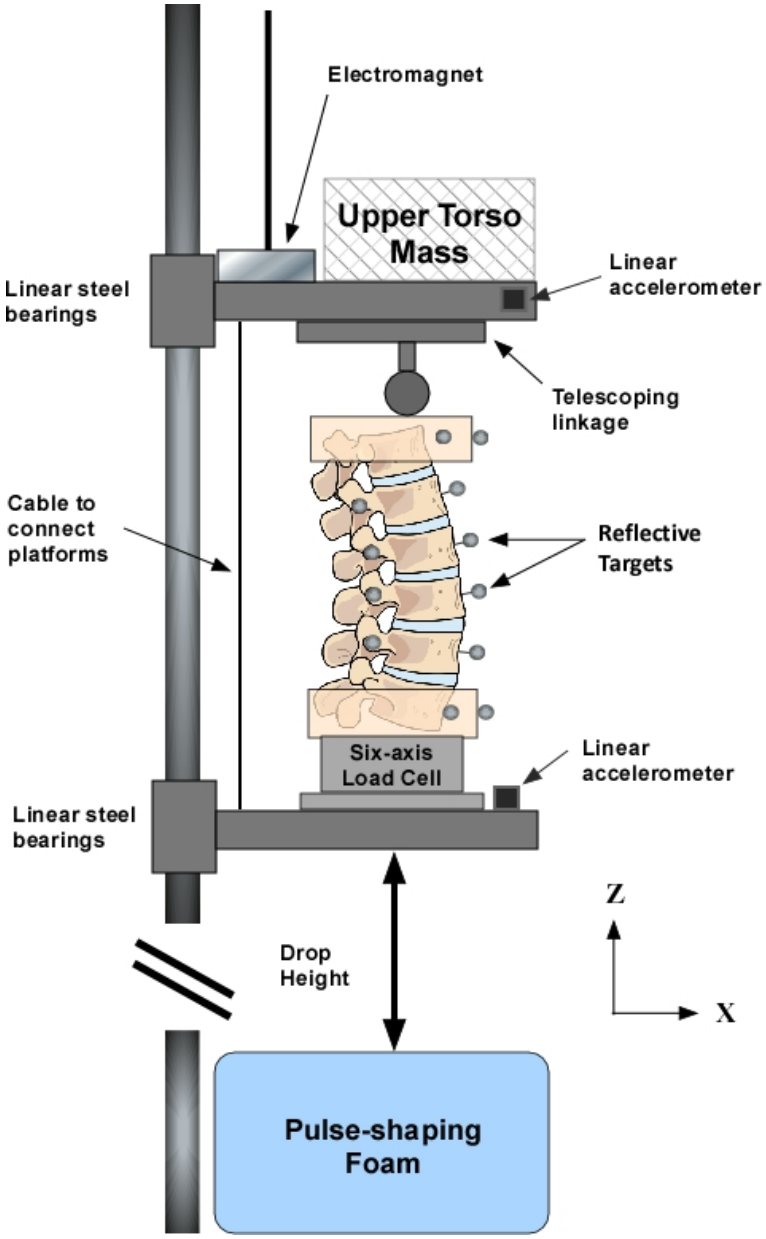

Figure 3: Experimental setup. Coordinate axes followed the right hand rule.

To impart axial loading, the entire apparatus, consisting of both platforms and the specimen, was raised to a specific height and held in place using an electromagnet. Mass was then added to the upper platform only after the electromagnet was holding the upper platform and the cable was holding the lower platform suspended. In this manner, the simulated mass did not preload the specimen. Upon manual trigger, the electromagnet released the entire apparatus which then was accelerated downward by gravity until the lower platform contacted the pulse-shaping foam. The *boost or in-rail* phase of a typical ejection sequence was simulated by decelerating ($+G_Z$) the lower platform with the foam. Since the upper and lower platforms were decoupled, as $+G_Z$ acceleration was applied to the bottom platform the upper platform applied a compressive inertial load to the superior end of the specimen.

2.2 Proof of Concept – Hybrid III Neck Segment

Prior to using human cadaveric specimens, initial testing was conducted to verify the experimental setup, accelerations, loads, and boundary conditions using a 50^{th} percentile Hybrid III anthropomorphic test device (ATD) neck segment. Details of the testing have been provided earlier [70]. A brief description follows. The neck segment consisted of five rigid plates interconnected by four rubber discs, for a total of four segmented levels. Three non-collinear kinematic targets were attached at each rigid segment to measure individual segment compressions. A mass was attached to the upper platform to simulate the appropriate upper torso mass of an average-sized male. The

loading cylinder was aligned with the center of the neck segment to apply compression loading. Several drop tests were conducted to characterize input acceleration pulses obtained through changing the drop height and the deceleration block (i.e., pulse-shaping foam). The key points are highlighted below.

It was discovered that using more compliant, resilient foam to decelerate the lower platform produced dynamic vertical acceleration pulses with temporal characteristics that approximated the *boost or in-rail* phase of an ejection sequence. Appropriate foam thickness was also determined. The mechanical details of the foam used for cadaveric testing are shown in Fig. 4. In general, initial drop height controlled maximum acceleration of the device (Fig. 5), and compressive properties of the pulse-shaping foam controlled the rate of acceleration onset and duration of the pulse. The same block of foam was sufficient to produce the acceleration pulses used for the test matrix outlined for cadaveric testing (Fig. 8).

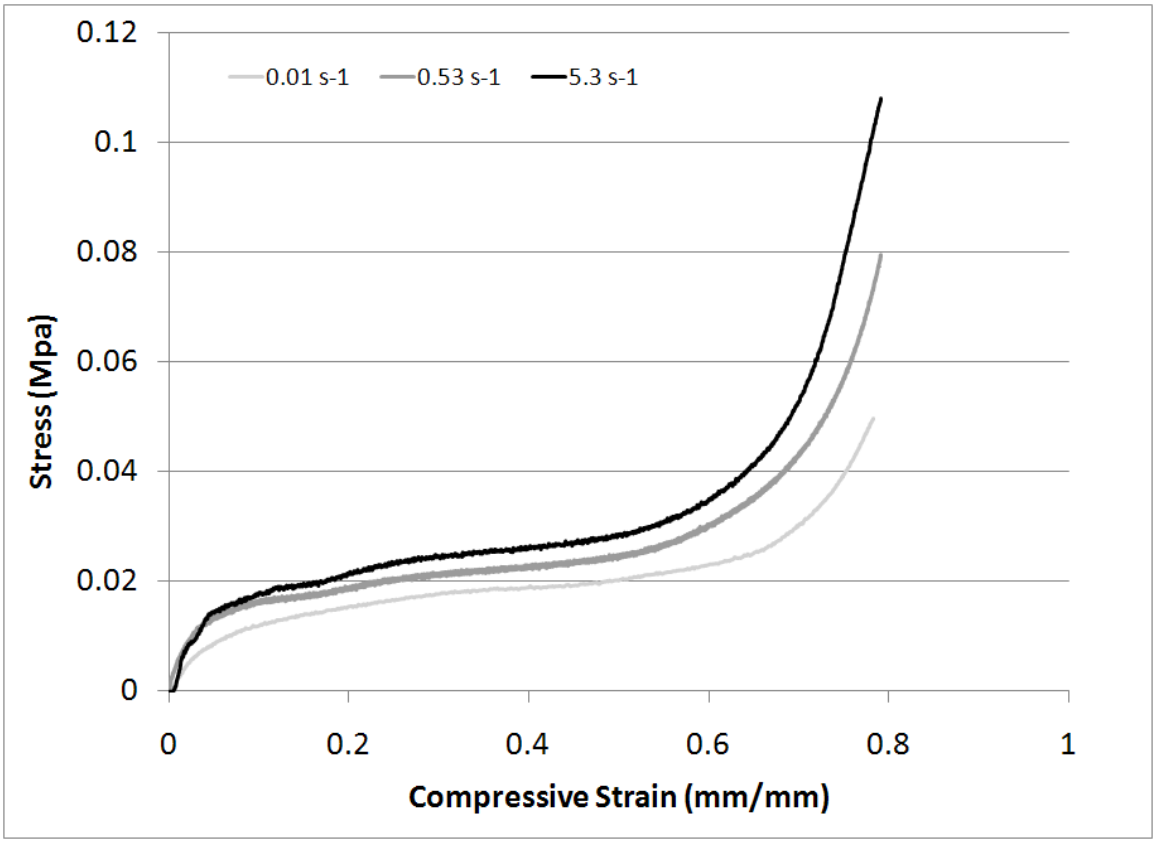

Figure 4: Compressive mechanical properties of the pulse-shaping foam. The foam dimensions were 30 x 45 x 65 cm (X,Y,Z) and had a density of 16 kg/m^2.

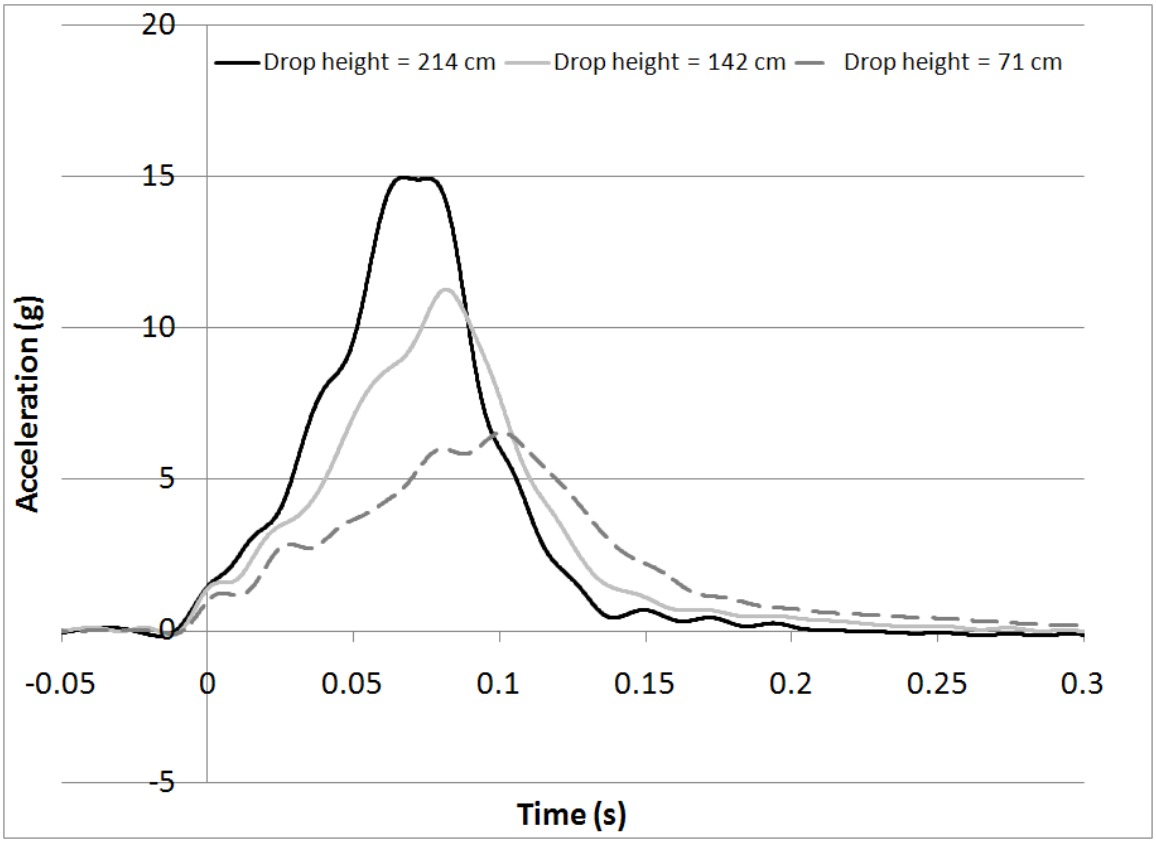

Figure 5: Acceleration pulses measured at the bottom platform for three separate tests. The magnitude of the pulses was scaled by changing the drop height.

Rate of acceleration onset was similar between the top and bottom platforms for any given drop test. The "dynamic response" was successfully simulated as evidenced by higher peak acceleration obtained by the top platform compared to the bottom platform (Fig. 6).

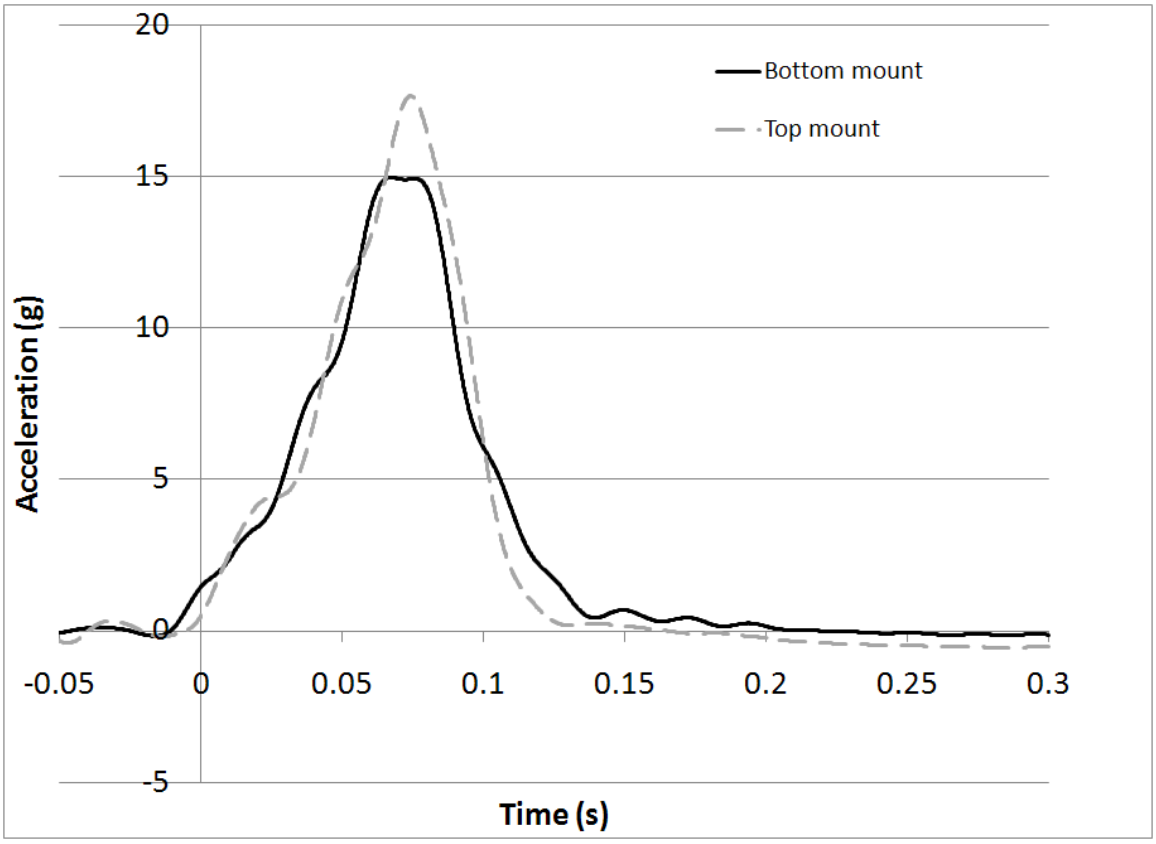

Figure 6: Representative platform acceleration versus time pulses for a vertical acceleration input simulating the *boost or in-rail* phase of a military seat ejection sequence using the neck segment.

For a vertical acceleration pulse approximating the *boost or in-rail* phase of a pilot ejection (Fig. 6), loads measured at the base of the neck segment during preliminary testing demonstrated approximately pure compression. Peak compressive force was 5.2 kN and anteroposterior and lateral shear forces were less than 100 N. Peak sagittal and coronal bending moments were less than 5.0 Nm. Thus, off-axis loads were considered negligible. Neck segment kinematics demonstrated compressive displacements at each level, and the setup was able to measure displacements at a resolution greater than 1 mm [70]. The experimental setup, accelerations, loads, and boundary conditions were investigated and verified. Thus, cadaveric testing was justified.

2.3 Specimen Information and Preparation

Four specimens were excised from PMHS that were free of Human Immunodeficiency Virus, and Hepatitis A, B, and C. The PMHS were also free of any spinal diseases or trauma. The PMHS were screened such that anthropometry and age approximated military aviators [7] as described in Table 3. Specimens were isolated at the twelfth thoracic vertebra (T12) and the fifth lumbar vertebra (L5). The T12 vertebra was isolated by transecting the T11-T12 intervertebral disc along with the facet joints at that level, and the ribs at T12 were removed at the costovertebral joints. All muscle, adipose, and other nonligamentous soft tissue were removed by dissection with caution to preserve the integrity of the ligaments, facet joints, and intervertebral discs. The specimens were wrapped in double plastic bags and frozen at -80^{o} C. Prior to testing, the specimens were thawed at room temperature for 12 hours and radiographs were taken to ensure that no abnormalities were present (Fig. 7). Computed tomography (CT) scans were also taken to compare pre- and post-test bony geometry (Siemens, Malvern, PA). Specimens were in flexion during CT scanning.

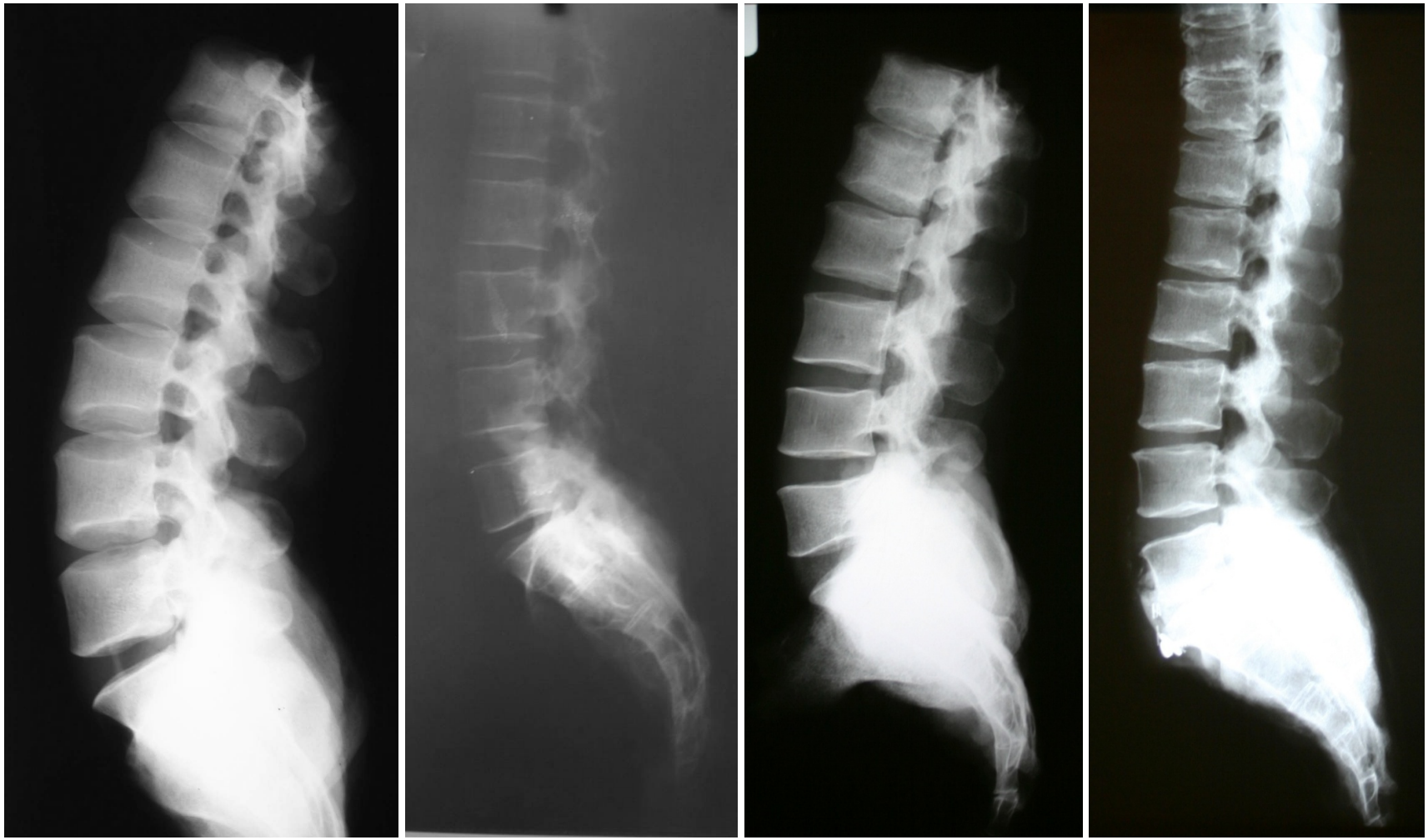

HS-657 **HS-591** **HS-673** **HS-530**

Figure 7: X-ray photos of specimens tested (General Electric Healthcare, Milwaukee, WI).

Table 3: PMHS demographics.

PMHS Number	Gender	Age (yr)	Height (cm)	Weight (kg)
HS-657	Male	26	173	100
HS-591	Male	37	180	114
HS-673	Male	33	188	113
HS-530	Male	45	175	100
Average Aviator	Male	37	177	78

The upper ¾ of T12 and lower ¾ of L5 were potted in polymethylmethacrylate (PMMA) to fix as much bone as possible without affecting soft tissues. The L2-L3 intervertebral disc was maintained horizontal during the fixation procedure to distribute lordotic curvature between upper and lower segments so as to minimize inter-specimen differences in overall sagittal orientation within the loading device. This was done to control the initial position in the absence of any good precedent.

2.4 Experimental Procedure

Each specimen followed the experimental test matrix outlined in Fig. 8. Due to the expensive cost of human cadaveric specimens, the test matrix was intended to minimize the number of specimens required. To comprehensively characterize the physiologic response of PMHS specimens, three tests were conducted well below failure thresholds prior to the Ejection test. This approach is supported by past studies comparing single and incremental trauma protocols in a burst fracture model [71-73]. The incremental trauma protocol was shown to produce statistically equivalent bony and

soft tissue injuries, represented by canal encroachment measurements and three-dimensional flexibility tests. Thus, specimens subjected to incremental trauma do not suffer greater soft tissue injury than those subjected to a single increased-severity trauma.

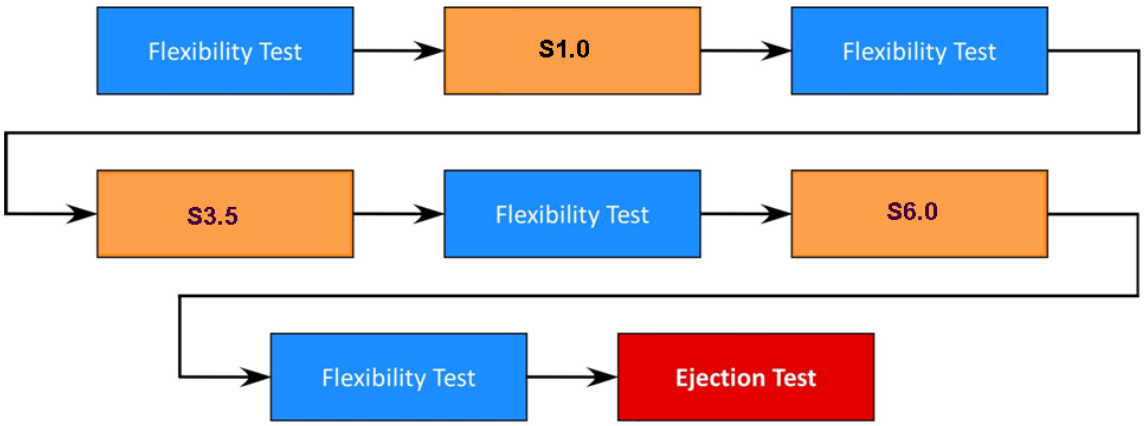

Figure 8: Experimental test matrix.

The first part of the test matrix subjected specimens to subfailure loading to outline spinal kinematics and assess repeatability of the model. Subfailure tests applied dynamic vertical (+Gz) acceleration with peak and rate of onset values below what was expected to result in spinal injury. This was achieved with a drop height of 61 cm. Mass (30.2 kg) was added to the upper platform to simulate the head, neck, thorax, and upper extremity mass of a 50th percentile male [74-76]. Three Subfailure tests were performed for each specimen with the inertial load from the upper platform applied at 1.0, 3.5, and 6.0 cm anterior from the posterior wall of the L3 vertebral body in the sagittal plane. These test conditions are referred to as S1.0, S3.5, and S6.0. These positions were chosen to constitute the Subfailure test matrix for several reasons. By conducting drop tests with the impacting cylinder at three eccentricities, more robust validation data

would be obtained that can be used to validate an ensuing computational model. The loading cylinder was placed anterior to the PLL of L3 for all tests so that only flexion moments were included in bending loads. The order of the testing protocol was established assuming that injury was more probable as the impacting cylinder moved anteriorly via the telescopic linkage, since it has been reported that compression force at failure in flexion was only 25% of that found in purely axial compression [77].

Since each specimen would undergo several insults, flexibility testing was included in the protocol to monitor structural integrity (Fig. 8). Prior to any testing, a baseline overall rotation of T12 relative to L5 was measured under a static 5 Nm flexion moment applied to the superior PMMA casting. The ROM motion parameter was documented. Although a pure moment was not applied, off-axis loads were minimized during application of the moment, and the ROM recorded in this manner was deemed sensitive enough to measure injury to the spinal column. Magnitude of the flexion moment used for flexibility tests was based upon literature. Pure-moment tests investigating bending responses of spinal segments typically apply between 4 and 10 Nm flexion/extension moments [78,79]. Thus, 5 Nm would suffice to flex the specimen and, still, remain within the physiological range [80].

Percent increase in flexibility was indicative of likely injury, and was expressed by the following equation:

$$\frac{\text{post-test flexion ROM - baseline flexion ROM}}{\text{baseline flexion ROM}}$$

Along with flexion flexibility tests, x-rays were taken between tests to confirm bony integrity and each segment was manipulated by hand by the same technician to obtain a qualitative assessment.

The second part of the test matrix consisted of drop tests designed to apply a $+G_Z$ acceleration pulse to the lower platform that approximated the *boost or in-rail* phase of a military seat ejection. It was presumed that this input acceleration was potentially injurious since spinal fractures were prominent in the clinical literature. This was achieved with a drop height of 168 cm. Specimens were initially preflexed with a 5 Nm load to bias the failure toward an anterior wedge fracture. The upper platform again approximated the mass of the head, neck, thorax and upper extremities of a 50^{th} percentile male. These test conditions are referred to as Ejection tests. Post-test CT scans were obtained of each specimen in a flexed position following the Ejection test to evaluate bony integrity.

2.5 Collection of Physiological Response Data

An eight-camera Vicon system (Vicon Corp., Oxford Metrics Group, Oxford, England) was used to collect three-dimensional kinematics of the vertebrae. Kinematic modeling in Vicon is accomplished using two environments: Workstation (version 4.5) and BodyBuilder (version 3.55).

Three non-collinear spherical targets (9.5 mm in diameter) were used to represent each vertebra. Three targets is the minimum requirement to define a plane and a complete segment in both position and orientation. From L1 to L4, a target was attached

to the anterior aspect of each vertebral body using 1 mm diameter pins and a target was glued to each transverse process. The targets were simply glued to the PMMA casting of T12 and L5 as shown in Fig. 3. Each set of three targets were defined in Workstation. Workstation was also used to record the kinematics at 1.0 kHz.

BodyBuilder was used for post-processing; to edit the original data and to apply a custom-written model script. Within BodyBuilder, the data was carefully edited to create a continuous trajectory for each target [81]. Target trajectories were used to reconstruct vertebral kinematics using the model script. The model script was written in BodyLanguage code, an interpreted programming language, which is read specifically by BodyBuilder to process the motion data and generate biomechanical outputs of interest. Within the script, each vertebra was modeled as a segment, and a local Cartesian coordinate system was created for each individual vertebra. Local axis origins were defined at the center of the vertebral body's posterior wall in the coronal plane with the x-axis directed anteriorly, the y-axis was directed to the left, and the z-axis was directed cranially. To calculate vertebral positions and orientations, local origins were aligned so that the x-y plane was parallel with the superior endplate. This was done by measuring distances and angles of the targets relative to the vertebra using lateral and anteroposterior radiographs. The Euler method was implemented to calculate three-dimensional orientation of each segment in the sequence XYZ.

Sagittal segmental angulation was computed for each motion segment (T12-L1 through L4-L5) as the flexion-extension angle of one vertebra relative to its inferior. Vertebral segmental angles (degrees) were filtered according to Channel Frequency Class (CFC) 60 specifications [82]. To monitor vertebral body anterior-wedge compression,

two additional targets (6.5-mm in diameter) were placed in the anterior wall of the body from L1 to L4 using 1-mm diameter pins, and oriented toward cranial and caudal extents on alternating right/left sides (Fig. 9). Vertebral body compression was calculated for each level as the relative vertical displacement between the two targets within the segment's local axis system, and data were filtered according to CFC 60 specifications. Vertebral body compression data can be used to identify the timing and extent of bony fracture.

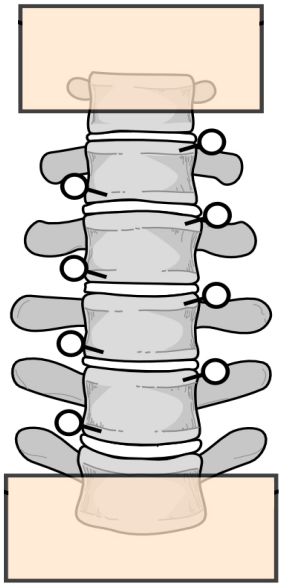

Figure 9: Orientation of Vicon targets to measure vertebral body compression. These markers are in addition to the markers used to define each vertebral segment.

Accelerations of upper and lower platforms were recorded at 10 kHz, and were filtered according to CFC 1000 specifications. Maximum acceleration (g) and rate of acceleration onset (g/s) of the lower platform were used to assess repeatability of the input acceleration pulse between specimens and test conditions, and can be used as an estimate of seat accelerations during actual military ejections. Rate of acceleration onset

was calcuated as the peak acceleration divided by the time duration between acceleration onset and the peak. Acceleration data of the upper platform quantified the dynamic overshoot of the superior end of the specimen.

Compression-distraction forces (N) and flexion-extension bending moments (Nm) were recorded at 10 kHz using the six-axis load cell, inertially compensated, transferred to the posterior aspect of the L5 vertebral body (Appendix A), and filtered according to CFC 600 specifications. Forces and moments were used to assess repeatability and demonstrate differences between the three subfailure loading conditions. These metrics were also used as injury tolerance predictors during tests.

CHAPTER 3: RESULTS

3.1 Specimen Evaluation

Each specimen was subjected to a minimum of four dynamic tests, with one specimen subjected to an additional two tests (total of six) to produce vertebral fractures.

For each test conducted, the initial segmental and overall (T12-L5) orientations of the specimens were measured (Tables 4-7). Level-by-level (segmental) orientations were output as the three-dimensional orientation of a vertebra within the axes system of the subjacent vertebra using the Vicon Bodybuilder model script. Radiographs were also taken of each specimen's initial position within the loading device prior to each test. All orientation measurements obtained using Vicon were confirmed with pre-test radiographs using the posterior tangent method [83,84].

Table 4: Initial sagittal orientation in degrees of specimen HS-657. Positive angles = flexion. Negative angles = extension.

	T12-L1	L1-L2	L2-L3	L3-L4	L4-L5	T12-L5
neutral position						
S1.0	-3.87	-2.94	-7.52	-11.98	-6.70	-33.00
S3.5	-4.11	-2.85	-7.44	-11.80	-6.64	-32.85
S6.0	-3.71	-3.23	-6.97	-12.95	-5.49	-32.35
pre-flexed position						
Ejection	-4.19	-0.73	-7.86	-10.56	0.42	-22.92

Table 5: Initial sagittal orientation in degrees of specimen HS-591. Positive angles = flexion. Negative angles = extension.

	T12-L1	L1-L2	L2-L3	L3-L4	L4-L5	T12-L5
neutral position						
S1.0	-2.78	-1.38	-3.82	-5.27	-8.58	-21.84
S3.5	-3.58	-0.84	-4.22	-5.4	-7.81	-21.85
S6.0	-2.55	-0.92	-4.26	-5.32	-8.18	-21.23
pre-flexed position						
Ejection	-1.28	0.64	-3.28	-3.35	-4.08	-11.34

Table 6: Initial sagittal orientation in degrees of specimen HS-673. Positive angles = flexion. Negative angles = extension.

	T12-L1	L1-L2	L2-L3	L3-L4	L4-L5	T12-L5
neutral position						
S1.0	-4.13	-1.02	-3.79	-4.85	-10.58	-24.37
S3.5	-3.87	-1.13	-4.04	-5.78	-9.11	-23.93
S6.0	-4.11	-1.37	-3.96	-5.35	-9.72	-24.51
pre-flexed position						
Ejection	-3.00	-0.86	-2.57	-4.80	-3.78	-15.02

Table 7: Initial sagittal orientation in degrees of specimen HS-530. Positive angles = flexion. Negative angles = extension.

	T12-L1	L1-L2	L2-L3	L3-L4	L4-L5	T12-L5
neutral position						
S1.0	-3.07	0.24	-2.27	-5.79	-10.19	-21.08
S3.5	-3.64	-0.06	-1.77	-5.39	-11.23	-22.09
S6.0	-2.28	-0.12	-2.30	-5.30	-10.85	-20.84
pre-flexed position						
Ejection	-0.12	1.14	-0.60	-2.29	-2.31	-4.19
1st Increased severtity	-1.39	1.36	0.96	-2.54	-2.40	-4.01
2nd Increased severity	-1.17	3.97	0.12	-3.97	-2.82	-3.88

The anteroposterior position of the loading bar in the sagittal plane was consistent among specimens for each test condition (Table 8). The positions were measured using pre-test x-rays that were taken with the specimens within the loading device (Fig. 10). The average loading cylinder position for each Subfailure testing condition corresponded well with the desired positions (i.e., 1.0, 3.5, and 6.0 cm anterior to L3 PLL). The loading cylinder in the sagittal plane was measured at approximately 5 cm anterior to the posterior wall of the L3 vertebral body.

Table 8: Average anteroposterior position of the loading bar relative to the midheight of the posterior wall of L3 and L5 for each test of the experimental test matrix.

Test	Distance (mm) anterior to L3 PLL	Distance (mm) anterior to L5 PLL
S1.0	11.4 ± 4.1	25.4 ± 3.2
S3.5	34.3 ± 4.3	49.5 ± 3.1
S6.0	55.0 ± 4.3	70.0 ± 3.9
Ejection	48.8 ± 6.2	

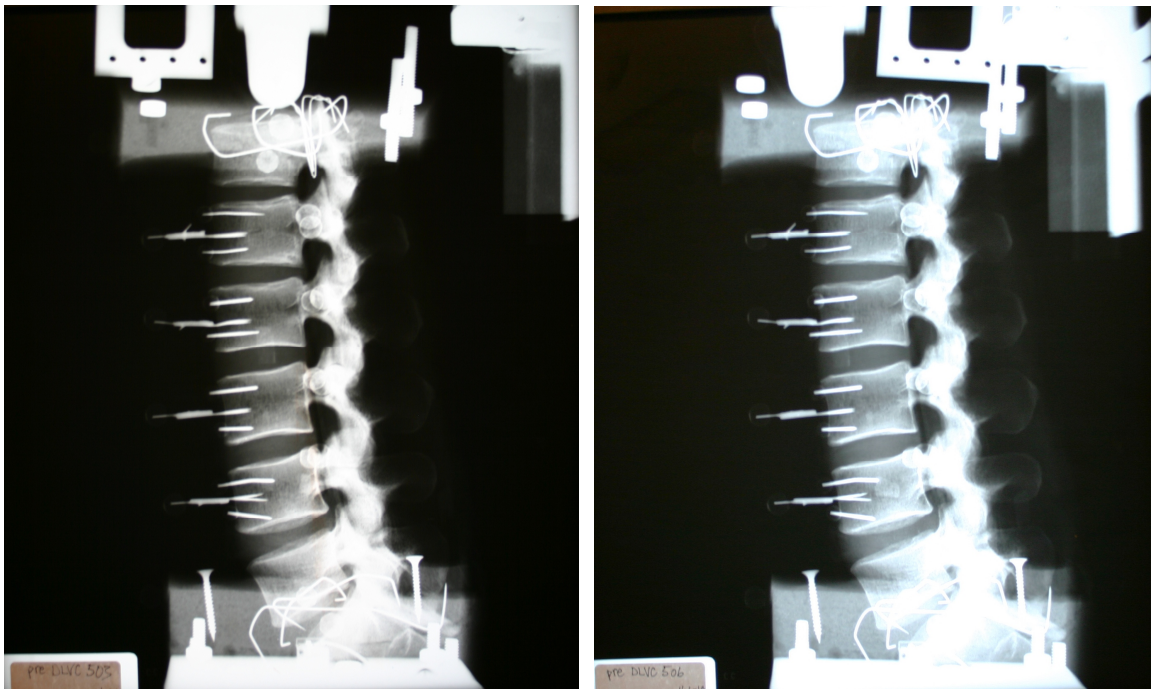

A B

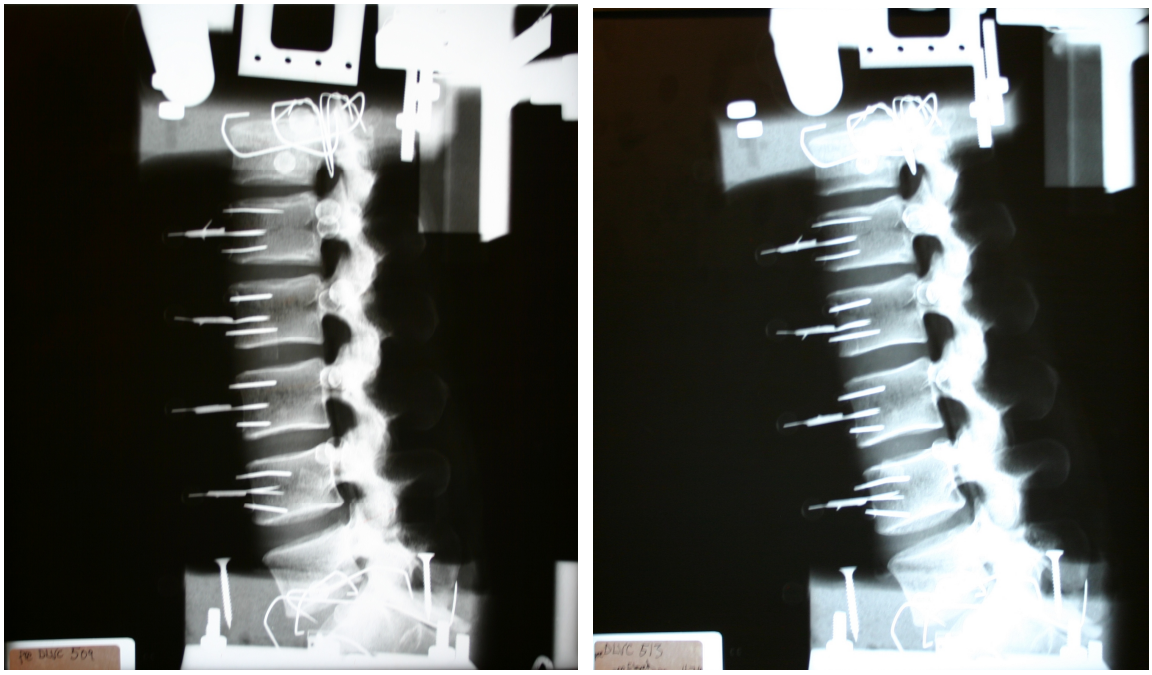

C D

Figure 10: Representative x-ray photos of specimen HS-673 showing pre-test specimen orientation and anteroposterior position of the loading bar for test series. (A: Test S1.0, B: Test S3.5, C: Test S6.0, D: Ejection test)

3.2 Subfailure Testing

Magnitude of peak lower platform vertical accelerations for test conditions S1.0, S3.5, and S6.0 were 6.1±0.4 g, 6.3±0.5 g, and 7.0±0.6 g, respectively. Rate of onset for lower platform accelerations for test conditions S1.0, S3.5, and S6.0 were 58.1±10.3 g/s, 55.7±10.2 g/s, and 72.3±4.1 g/s, respectively. Physiological response data are summarized in Table 9. A representative time-based loading history of these data is included in Figure 11.

Table 9: Summary (mean ± standard deviation) of response data for Subfailure testing.

	S1.0	**S3.5**	**S6.0**
Upper platform peak acc.(g)	6.9 ± 0.7	7.0 ± 0.4	7.4 ± 0.6
T12-L1 (degrees)	-3.3 ± 0.7	5.3 ± 0.6	6.1 ± 2.7
L1-L2 (degrees)	-3.4 ± 0.6	3.6 ± 0.5	4.6 ± 1.1
L2-L3 (degrees)	-2.5 ± 0.5	1.7 ± 2.2	4.8 ± 0.7
L3-L4 (degrees)	-1.9 ± 0.6	-1.5 ± 0.9	1.0 ± 1.6
L4-L5 (degrees)	5.9 ± 0.9	-0.6 ± 2.7	-3.5 ± 0.6
Compressive force (Fz; N)	1874 ± 107	1868 ± 59	1865 ± 95
Shear force (Fx; N)	-47 ± 99	-340 ± 86	-603 ± 154
Flexion moment (My; Nm)	45 ± 3	31 ± 8	21 ± 6

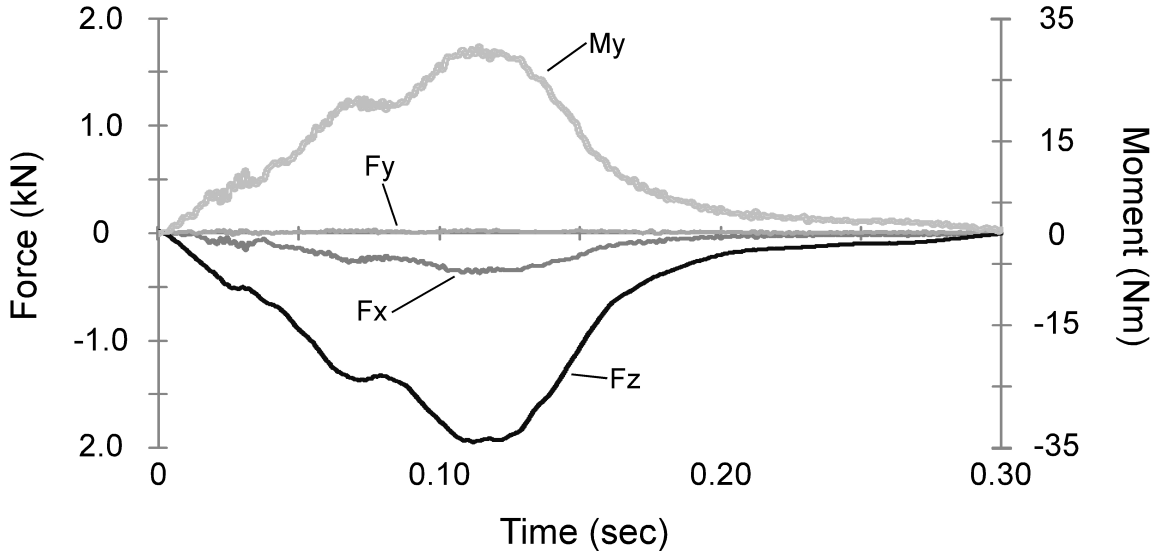

Figure 11: Representative time-based loading history for test condition S3.5.

Note: Kinematic data were not included for specimen HS-673 during the S3.5 Subfailure test condition. Therefore, mean kinematic data for test condition S3.5 represent only three specimens.

Dynamic kinematics of the lumbar spine demonstrated first order buckling during all Subfailure tests [85]. Condition S1.0 resulted in mean extension at T12-L1 through L3-L4 levels with flexion at the caudal-most level (Fig. 12). The specimens demonstrated opposite curvature as the loading cylinder was moved anteriorly. Condition S3.5 resulted in mean flexion at T12-L1 through L2-L3 levels and mean extension at L3-L4 and L4-L5 levels. Condition S6.0 resulted in mean flexion at T12-L1 through L3-L4 levels and mean extension at L4-L5. Specimen-to-specimen repeatability of segmental kinematics was considered to be acceptable (Fig. 12).

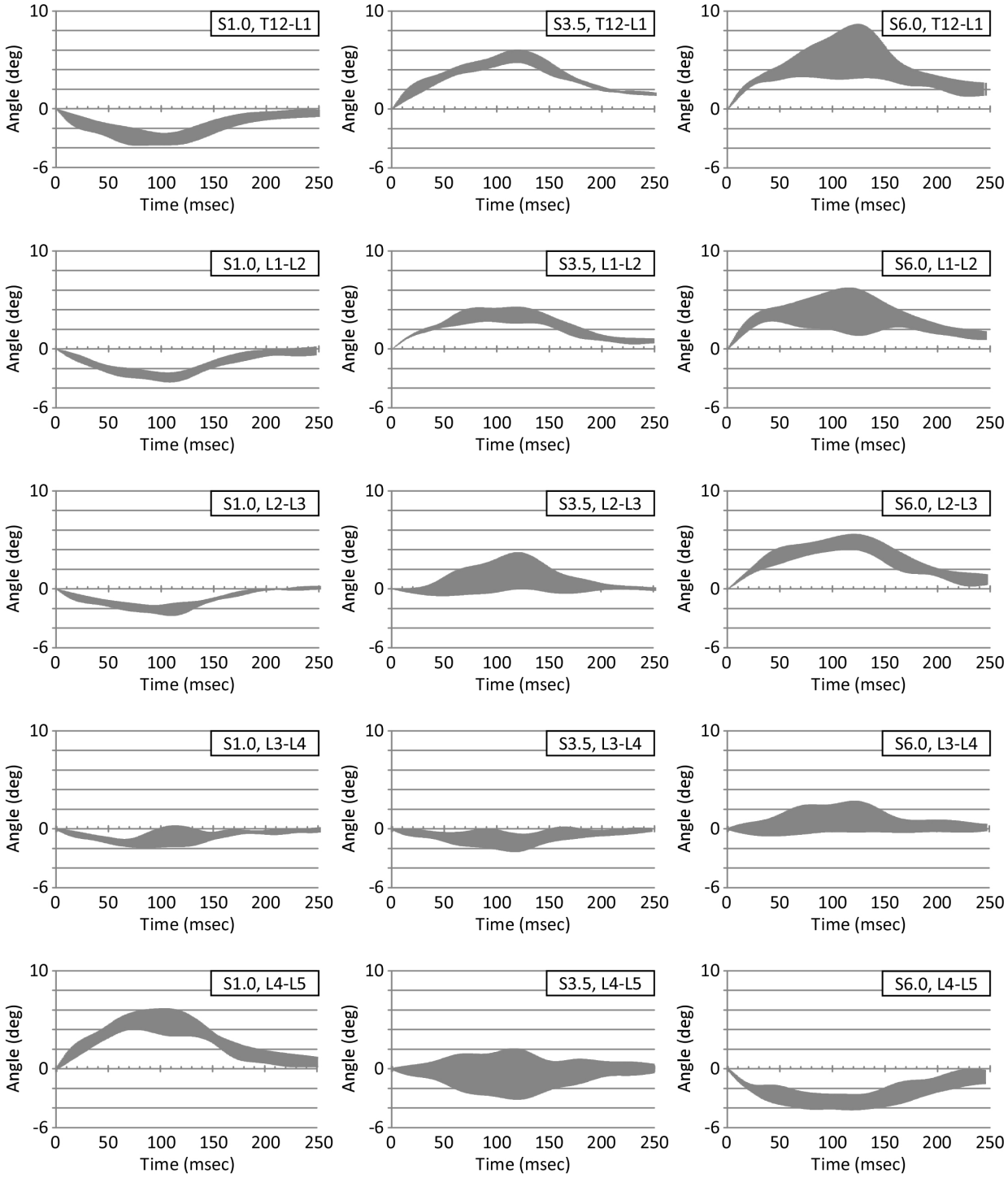

Figure 12: Segmental kinematics obtained from subfailure testing (flexion: positive; extension: negative).

The mechanical integrity of the specimens was assessed during Subfailure testing using a number of metrics. Post-test inspection of each specimen did not reveal evidence of soft tissue or bony failure. Static assessment of T12-L5 flexion flexibility indicated that soft tissue failure was unlikely. Dynamic compression of the vertebral bodies revealed that bony fracture was unlikely as relative vertebral body compressions did not exceed 3.3% across all Subfailure tests. Flexion flexibility tests were conducted after every test to identify soft-tissue subfailures that may have occurred during dynamic testing. These responses were compared to baseline flexion rotations to identify possible injury (Table 10). Baseline flexibility for the four specimens was 7.7±1.3 degrees in response to a 5 Nm flexion moment. For three specimens, overall static T12-L5 flexion increased by less than 12% following each of the three dynamic tests compared to the magnitude of flexion obtained prior to dynamic testing. For HS-673, overall static T12-L5 flexion increased by 24% following the S3.5 test. However, increased flexibility following the S3.5 test for that specimen was likely not indicative of soft tissue failure as flexibility decreased by 11% following the subsequent dynamic test (S6.0).

Table 10: Sagittal flexion flexibility test results. The specimens were flexed with a 5 Nm load, and the overall change in rotation (ΔT12-L5) compared to baseline was recorded in degrees using Vicon.

HS-657	pre-S1.0	pre-S3.5	pre-S6.0	post-S6.0
Δ T12-L5	8.21	8.46	8.22	9.02
HS-591	pre-S1.0	pre-S3.5	pre-S6.0	post-S6.0
Δ T12-L5	6.69	6.97	7.52	7.14
HS-673	pre-S1.0	pre-S3.5	pre-S6.0	post-S6.0
Δ T12-L5	6.5	6.51	8.07	5.77
HS-530	pre-S1.0	pre-S3.5	pre-S6.0a	post-S6.0
Δ T12-L5	9.26	9.42	9.18	9.64

3.3 Failure Testing

Following Subfailure testing, each specimen was subjected to a single drop test designed to apply the vertical acceleration pulse from the *boost or in-rail* phase of a military seat ejection sequence to the lower platform. The mean peak lower platform vertical acceleration for the four ejection tests was 14.8±1.7 g. The mean rate of onset for the four tests was 178.9±11.3 g/s. Maximum compressive forces and flexion moments were 4581±121 N and 84±26 Nm (Fig. 13). The experimental setup applied compression-flexion loading as evidenced by the negligible y-axis forces measured (Fig. 13).

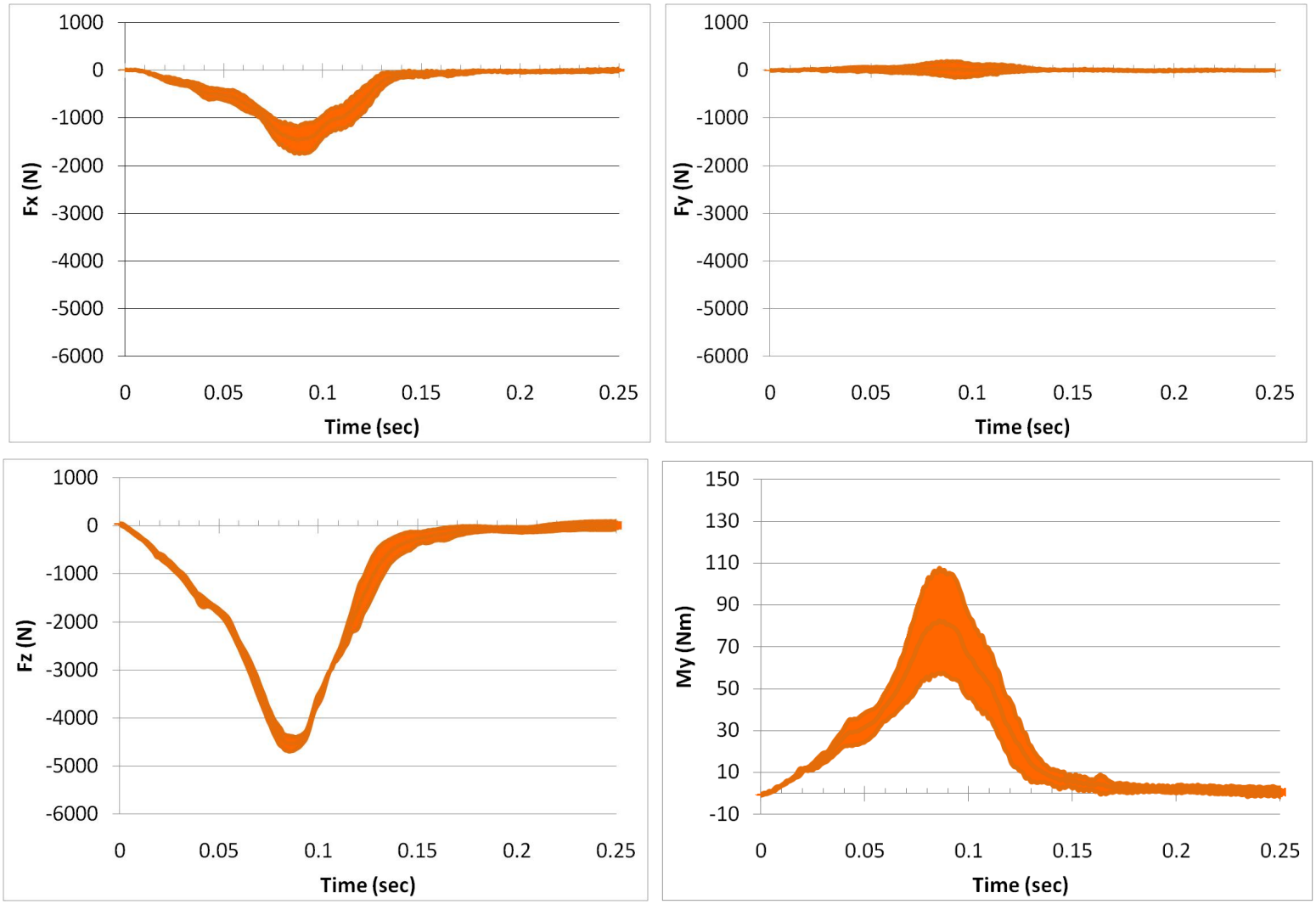

Figure 13: Loading corridors of the four specimens obtained from Ejection tests. The corridors represent the mean experimental response ± one standard deviation.

Analysis of dynamic vertebral body compressions at L1 through L4 revealed that compressions did not exceed 4.1% during Ejection tests. This indicated that catastrophic compressive fracture likely did not occur. Soft-tissue injury was unlikely as well. Post-test flexion flexibility of HS-657, HS-591, HS-673, and HS-530 increased 19.6%, 15.7%, 11.2%, and 1.1%, respectively. Furthermore, segment manipulation by hand did not qualitatively identify any specific tissue failure during post-test inspection of the specimens.

Table 11: Sagittal flexion flexibility test results. The specimens were flexed with a 5 Nm load, and the rotation (ΔT12-L5) was recorded in degrees using Vicon. Pre-Increased severity-1 rotation is data for post-Ejection test of specimen HS-530.

HS-657	pre-Ejection	post-Ejection	
Δ T12-L5	9.02	9.85	
HS-591	pre-Ejection	post-Ejection	
Δ T12-L5	7.14	7.74	
HS-673	pre-Ejection	post-Ejection	
Δ T12-L5	5.77	7.23	
HS-530	pre-Ejection	pre-1st Increased severity	pre-2nd Increased severtity
Δ T12-L5	9.64	9.36	11.11

Because no specimen sustained identifiable vertebral fractures during the Ejection tests, one specimen was subjected to two additional increased-severity tests (increasing peak acceleration and rate of onset). This was done to validate the clinical relevance of the current experimental model and to generate injury data. Only the input acceleration to the lower platform was changed; all other aspects of the experimental boundary conditions remained the same. The chosen specimen (HS-530) demonstrated the smallest

increase in flexibility following the previous Ejection test. The first increased-severity test applied a maximum acceleration of 16.4 g with 329 g/s rate of onset to the lower platform. This was achieved by raising the drop height to 198 cm. The maximum compressive force during that test was 4,620 N; the maximum bending moment was 112 Nm flexion.

Since the post-test inspections of the specimen's mechanical integrity did not reveal evidence of bony fracture, the specimen was subjected to a second test of increased severity. The second increased-severity test applied a maximum acceleration of 21 g and rate of onset of 488 g/s. This was achieved by increasing the stiffness of the foam block while maintaining drop height at 198 cm. The maximum compressive force during the second increased-severity test was 6,106 N; the maximum bending moment was 168 Nm flexion. Dynamic vertebral body compression data and post-test inspection identified bony injury, so no further tests were conducted.

Dynamic vertebral body compressions during the second and final increased-severity test approached 60% at the L4 level. Vertebral body compressions at the L2 and L3 levels were less than 20% (Fig. 14). L1 body compression data was not obtained due to the superior PMMA fixation occluding Vicon targets from the cameras during dynamic flexion of the specimen. CT scans were obtained of HS-530 in the flexed position following the test. Post-test CT confirmed the presence of an anterior wedge fracture at L4 and a burst fracture at L1 (Fig. 15).

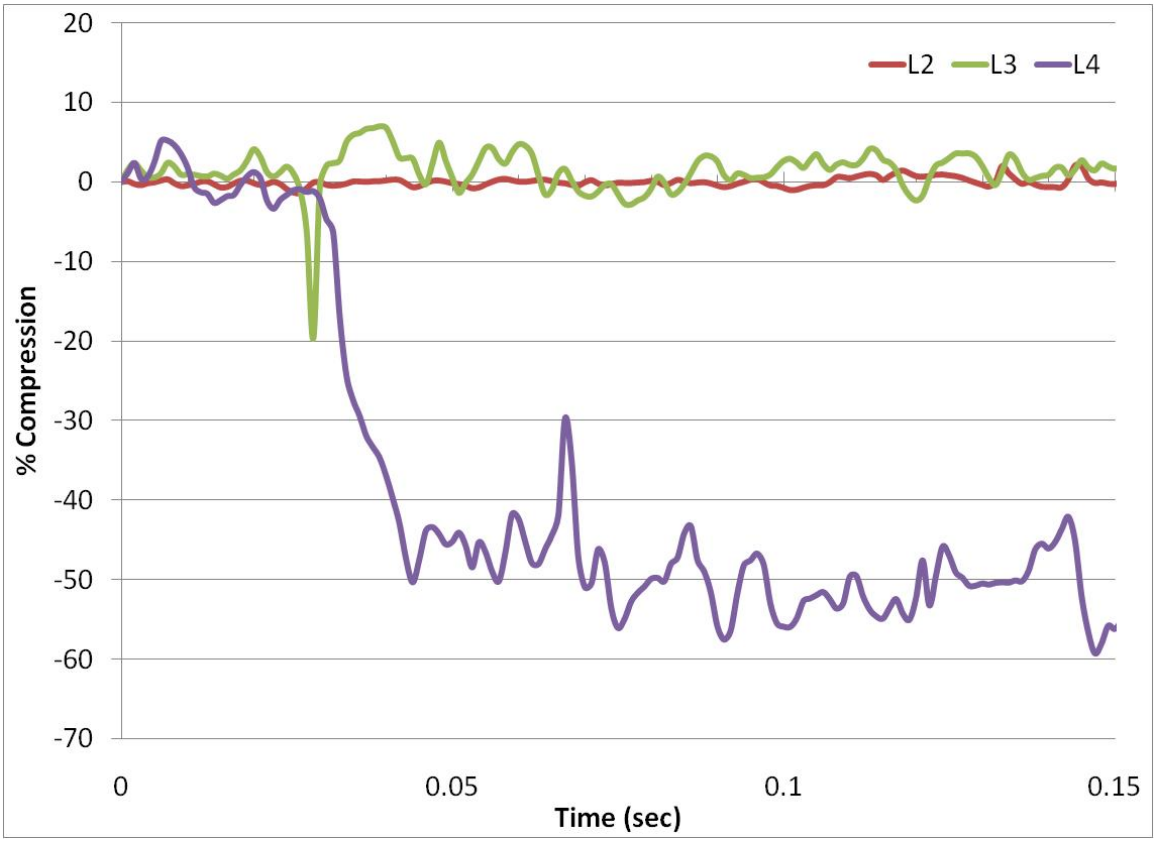

Figure 14: Percent vertebral compression following the final higher severity vertical pulse.

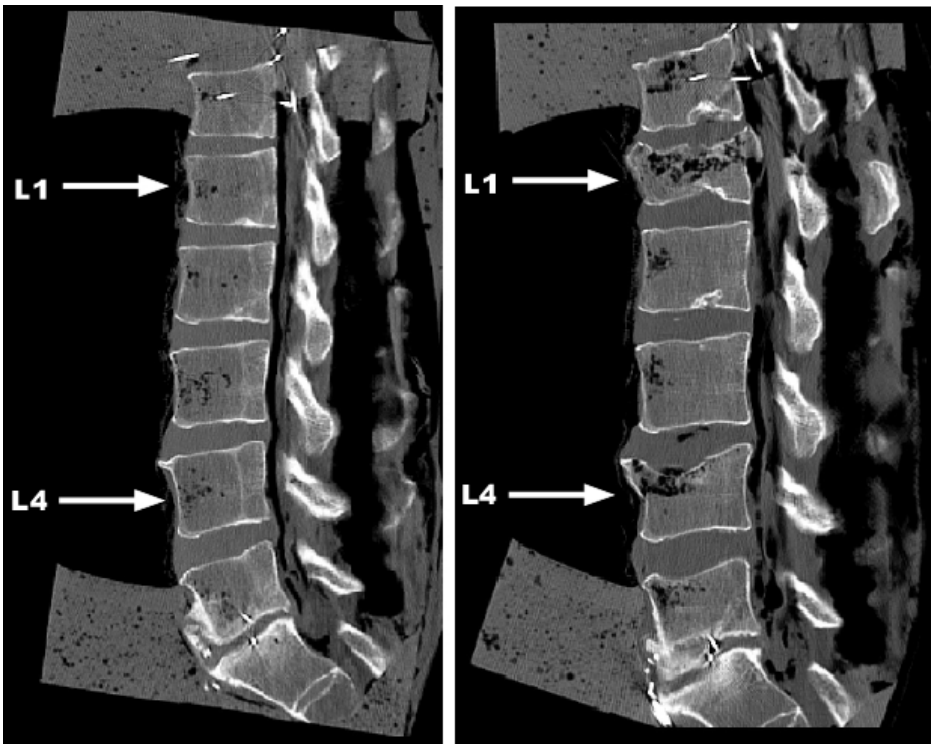

Figure 15: Pre-testing sagittal CT of specimen HS-530 (left). Post-testing sagittal CT of specimen HS-530 following final increased-severity vertical acceleration pulse (right). The CT slices are presented at approximately the same medial-lateral position. The CT image on the right demonstrates a burst fracture at L1 and an anterior wedge fracture at L4.

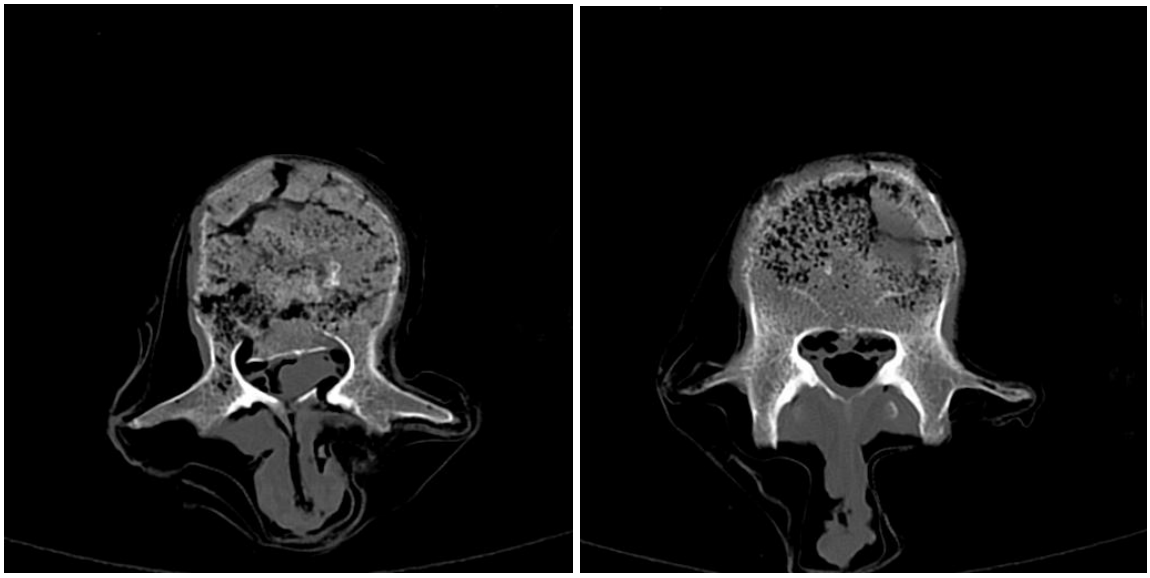

Figure 16: Axial CT of specimen HS-530 following final increased-severity vertical acceleration pulse demonstrating laminar fracture at L1 (left) and intact posterior column at L4 (right).

CHAPTER 4: DISCUSSION

4.1 Discussion of Subfailure Results

4.1.1 General Discussion

A biomechanically accurate model was developed to fully understand injury mechanisms and characteristics of a military seat ejection from an aircraft. The experimental model quantified metrics associated with injury tolerance including the magnitude, rate, and duration of applied accelerations, and resultant loads and kinematics.

Subfailure tests' loads were well below failure thresholds reported for whole lumbar spines, and no fractures occurred. Duma et al. reported concurrent failure loads of 5,009 N compression and 237 Nm bending moment [18]. Peak compression force and flexion moment during Subfailure testing did not exceed 1,993 N and 47 Nm, respectively. Lack of bony injury was confirmed by post-test radiographs. Kinematic corridors were obtained under several boundary conditions to provide robust validation data for ensuing computational models of the thoracolumbar spine. The initial overall (T12-L5) sagittal orientation of each specimen remained consistent throughout the Subfailure tests (Table 4-7).

Flexibilities of the specimens were measured when intact and after each successive test to ensure that no soft-tissue (or bony) injuries occurred. Increased flexibility following a drop test would be indicative of injury. Maintaining that level of

increased flexibility following successive tests would confirm injury. The measurements in the current study were well below flexibility increases reported by Panjabi et al. for injured spinal specimens [64,86]. Under applied flexion moment, the flexibility of specimens following burst fractures increased significantly from the intact values by 123% [86]. Subject to an incremental trauma protocol, injury was determined in specimens by a flexion/extension flexibility increase of an average of 57% [64]. Thus, none of the specimens were decisively injured during the Subfailure tests. Post-test segmental manipulation and radiography further confirmed the integrity of the specimens following all Subfailure tests.

Full column lumbar spines were used in the current study to incorporate correct anatomic boundary conditions in addition to the realistic loading in the experimental set up. Although first order buckling occurred, the pattern and magnitude of sagittal plane motions were very repeatable with the highest level of variability at the inflection point. This experimental phenomenon is common in longer-length specimens that are unconstrained during axial loading [87]. In the past, studies exercising the MTS or weight-drop techniques have regularly used three-vertebra segments. This approach does not account for the effects of longitudinal ligaments or the curvature of the spine [59,79], both of which affect characteristics of thoracolumbar fractures [88,89]. When larger PMHS segments were used, past researchers biased the fracture site by leaving only one vertebra exposed during traumatic loading [16,71] or by creating a stress riser on the anterior cortical shell of the body of the vertebra-of-interest prior to traumatic loading [22,90]. By using a full intact column, unbiased fracture sites were obtained in the current study (refer to Section 4.2.1).

4.1.2 Application to Validating Computational Models

The experimental response corridors obtained herein may prove valuable to validate a finite element (FE) lumbar spine model. One way to quickly and adequately improve aviator safety devices is to use computational models to conduct parametric studies investigating the lumbar spine tolerance. Before this can be done, the computational model must first be validated with respect to experimental data under the same boundary conditions to verify that the response is physiologic. Currently, there are no dynamic-response data of the thoracolumbar spine under this mode of loading that can be used for this purpose. Once a computational model is developed and validated, it is conceivably the most economical research methodology available [91]. A computational model offers absolute repeatability and provides ease for parametric studies to identify particular changes in the outcome measure due to varying any input parameter. It is the most efficient way to test prevention techniques and advance our understanding of mechanisms of injuries.

Dynamic computational models of the spine have been used to investigate seat ejection since the middle of the twentieth century. Early models of the spine simply consisted of an elastic or visco-elastic rod, free at the superior end while the other end was subjected to a prescribed axial acceleration pulse [63,92]. The amount of simplification in these continuum models is obvious. Lumped models were also common [61,93,94], and helped further characterize ejection tolerance. However, most authors noted that a better understanding of the actual physiological response would greatly

approve the models to be more suitable for injury prediction and mitigation. This type of data could only be obtained through experimental work.

One example feat was the experimental work by Prasad et al. [95]. This work provided evidence that axial loads passed through both the vertebral body via the intervertebral disks and the lamina via the facet joints. The loading history attested that all computational models at the time were not accurately simulating the actual spinal response since two load paths were not accounted for. In 1974 Prasad and King validated a discrete parameter model of the spine by using the experimental data derived from 18 $+G_Z$ tests using 3 full-body cadavers [95,96]. The end conditions for the mathematical and experimental simulations were matched, and the facet and intervertebral loads predicted by the model were compared to the loads measured in the cadavers. The two studies in tandem highlighted the importance of validating computational models against experimental data which was not commonly done prior to this date.

Similar to the experimental loading data that was paramount in validating the updated discrete parameter model of the spine in 1974, the kinematic data of the current study should be instrumental in advancing future FE models to investigate military seat ejection. This is the first study to measure segmental and overall kinematic corridors of the lumbar spine under high rate axial loading. The loads exerted by the specimen onto the lower platform were also measured. The different loading eccentricities should provide robust validation data that can be used to calibrate nominal levels of a whole lumbar spine FE model.

Cadaveric kinematic data has been utilized widely in the past to extensively validate computational models. For example, Stemper et al. validated a MADYMO

head-neck computational model so that the model could be employed to investigate whiplash biomechanics in greater detail [97]. The group used experimental data obtained from ten PMHS head-neck complexes to produce validation corridors, consisting of global (head-T1 angle), segmental, and local (resultant facet joint motion) kinematic responses (mean experimental response ± 1 standard deviation). The boundary conditions and loading of the computational model were matched to the experimental, and the model was considered validated if its response fell within the experimental corridors. Guan et al. validated a clinical FE model of the human lumbosacral spine using kinematic corridors as well [98]. The group validated moment-rotation responses of the FE model by comparing the predictions to in vitro data using the same range of loading. Likewise, validating an ensuing FE model of the intact lumbar spine by comparing multiple outputs against a range of input parameters (i.e., S1.0, S3.5, and S6.0 loading eccentricities) will provide a greater degree of confidence in the model's results.

4.2 Discussion of Failure Results

4.2.1 General Discussion

Historically, the most popular method used to investigate burst fractures has been the weight-drop method. The input measure of interest was impact energy, or simply the potential energy of the falling mass. An initial burst fracture threshold was determined to be 94.2 J [71]. While an energy threshold is useful for the weight-drop injury model, it is less constructive in understanding the injury mechanism and ultimately defining an injury

criterion for burst fractures because it does not take into account the duration or rate of energy transfer. In the current study, over 450 J was imparted on four separate specimens in a similar fashion without producing a burst fracture. Rather than simply an energy quantity, external measures of the loading environment (e.g., acceleration magnitude and rate of onset, axial force, and flexion-extension moment) are more applicable to understanding injury causation. Our experimental setup allows easy control of many input parameters that directly affect injury risk and severity – the axial acceleration pulse applied to the spine, the compression force, the extension-flexion moment, and initial orientation of the specimen. Moreover, our setup applies +Gz acceleration to the pelvis and generates inertial loading on the thoracolumbar spine. This is a realistic loading scheme for ejections – acceleration application at the pelvis and reaction load at the superior end of the spinal column.

For the Ejection tests, the specimens were preflexed with a 5 Nm load to bias the results toward an anterior wedge fracture. As the spine is flexed the facet joints bear a lower share of axial load, and stresses increase in the anterior column causing the spine to be less resistant to compressive loading [99-101]. Experimental tests have provided evidence for this assertion wherein preflexed specimens had a lower compressive tolerance [11,19,102]. Although spinal posture largely affects the distribution of load amongst the tissues of the spine, concurrent dynamic flexion will not change the site of injury from the vertebra to the intervertebral disc when peak compression magnitudes exceed 50% of a spinal level's compressive strength [103]. Thus, using a preflexed posture for the ejection tests was warranted given the magnitude of compressive loading.

Since no compression fracture was produced in any of the specimens by the initial Ejection test an incremental trauma approach was used for the additional increased-severity tests using one of the four specimens to produce a bony injury. An incremental trauma approach was used because it is superior to the single trauma approach in determining an injury criterion [71].

The present study induced spinal fractures in only one specimen since the primary purpose was model development. The Denis classification scheme was used to classify the thoracolumbar fractures in the current study [29]. It is currently the most widely referenced classification in experimental biomechanics literature. The scheme describes the fracture pattern and mechanism, and proposes clinical instability based on the three-column theory. The three columns include the anterior, middle, and posterior columns (Fig. 17). According to Denis, injury occurring to two or three of the columns results in instability. Furthermore, Denis emphasizes that the middle column is the key contributing factor to clinical instability. Panjabi et al. supported this assertion later in 1995 and provided biomechanical evidence that the middle column was the primary determinant of mechanical stability of this region of the spine [11]. In the present context, clinical instability is defined as the inability of the spine under physiological loads to maintain relationships between vertebrae so that there is neither initial nor subsequent neurologic deficit/major deformity/severe pain [11].

The specimen subjected to the second and final increased-severity vertical acceleration pulse sustained a type-A burst fracture at L1 (Fig. 15). All three columns of the spine were disrupted at his level. Comminution of the entire vertebral body occurred resulting in fracture of both end plates and retropulsion of body fragments into the

vertebral foramen. Jelsma et al. reported that the fragment of bone impinging on the spinal cord due to a burst fracture most commonly resulted from the posterior-superior corner of the vertebral body [104]. The current experimental model produced similar results (Fig. 15). The left lamina was also fractured (Fig. 16). A type-B compression fracture was also sustained at L4 (Fig. 15). The mechanism of fracture was anterior flexion, resulting in the most frequent type of compression fracture, failure of the anterior aspect of the upper end plate. The posterior wall of the body, pedicles, and lamina remained intact (Fig. 16). Thus, the vertebral foramen had not been transgressed and there was probably no neurological insult at that level.

Figure 17: The spine is divided into three longitudinal columns according to the three-column theory. The anterior column includes the anterior longitudinal ligament and the anterior two-thirds of the body and disc. The middle column includes the PLL and the posterior one-third of the body and disc. The posterior column includes the posterior ligament complex, pedicles, lamina, and facet joints.

Only two past studies have used full intact columns to investigate thoracolumbar injuries [18,60]. Both studies used the MTS technique. Yoganandan et al. tested intact C2-, T2-, T3-, T4-, and T6-L5 columns in quasistatic compression-flexion loading and produced over 38% of the failures at levels T12 and L1. Duma et al. dynamically tested two T12-L5 segments and both failures occurred at T12. These results are similar to the current study, wherein the primary injury also occurred within the thoracolumbar junction, and are noteworthy for comparison.

Axial acceleration of 21 g and rate of onset of 488 g/s produced fractures at L1 and L4. Multiple level spinal injuries are indicative of more severe trauma loading. When multiple level noncontiguous spinal injuries occur, literature has recognized definite patterns of injury [105,106]. One of the patterns includes having primary fractures at T12-L2 with associated secondary fractures at L4-L5. The primary injury is defined as the injury first identified which accounts for the patient's pain, symptoms, instability, and neurologic deficit. The secondary injury is defined as the less severe injury which has less neurologic and stability significance. The current model, incorporating realistic loading boundary conditions, produced the common fracture pattern stated above that is commonly seen in the real world. Multiple level spinal injuries are also common in injured ejectees, although the injury patterns are not documented well in literature [2,5,6]. For example, in the Republic of Bulgaria from 1953 to 1993, 25% of aircrew that sustained fractures had multiple level fractures.

Most serious injuries due to ejection are in the form of a vertebral fracture, most commonly occurring at the thoracolumbar junction [2,4,9,10]. Recent ejection data, lumping aircraft and performance envelope types, indicate that between 19.5% and 60%

of sustained vertebral fractures by survived ejectees occur at T12-L5 [6-8]. Burst fractures, specifically, predominantly affect the thoracolumbar junction. Large-scale cohort studies reported that more than 83% of burst fractures occur between T12-L5 [29,36,37,107]. These reports validate the clinically-relevant injury obtained in the current study.

Comparable axial traumatic loading situations produced similar injury outcomes to the current study as well. For example, an improvised explosive device attack to an armored (mine-resistant ambush-protected) vehicle produced an L1 burst fracture and L4 compression fracture in one soldier [108] – trauma similar to the injury produced in the current study. Other examples including axial spinal loading due to helicopter crashes, motor vehicle crashes, parachute jumping, and falls from height produced like vertebral fracture frequency distributions with modes at T12-L1 [109-112]. Therefore, although the injury model was focused on injuries sustained during ejection, the current model can also be used to study other typical axial loading scenarios since the injury patterns are consistent and loading/boundary conditions of the setup are flexible.

It is important to note that the initial phase of an ejection sequence, the *boost or in-rail* phase, was simulated in the current study. A noteworthy difference between this model and an actual military seat ejection is the duration of the vertical acceleration pulse. The mean experimental acceleration pulse that was input for the Ejection tests (< 150 ms) was shorter in duration than acceleration pulses measured on contemporary ejection seats (> 300 ms). However, this difference in duration is thought to play a secondary role in the production of vertebral injuries described in the current study. Specifically, timing of the L1 burst fracture and L4 anterior wedge fracture indicated that

both injuries occurred during the initial acceleration onset. Thus, it may only be necessary to match the rate of onset and peak acceleration of the experimental pulses with the real-world accelerations measured.

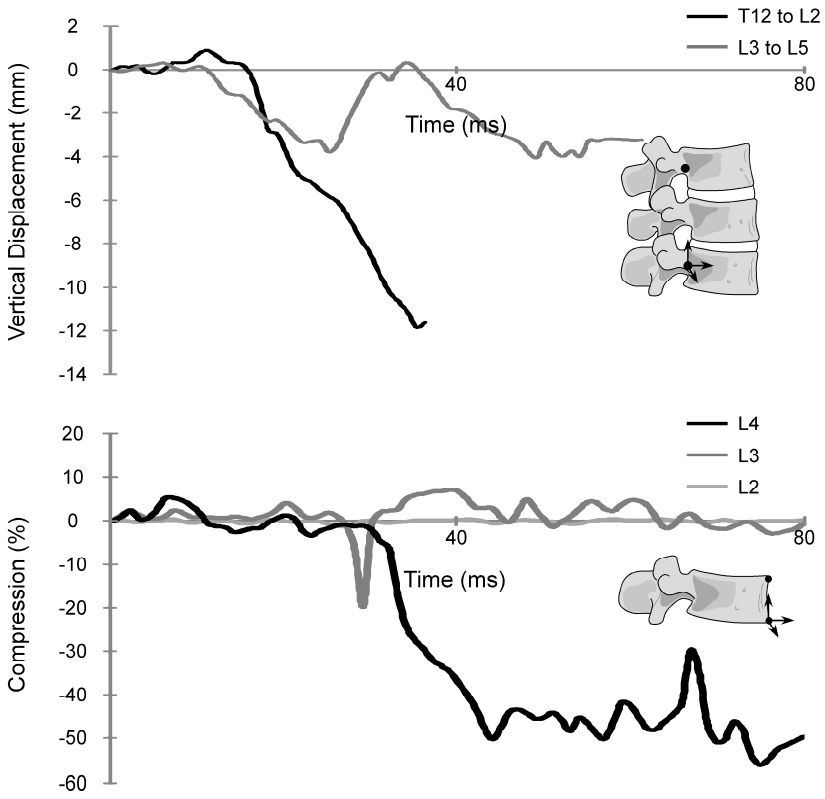

Figure 18: Time-history plots of injury data obtained during 2nd Increased-severity test. The top figure displays the relative vertical displacement of upper and lower lumbar segments during the onset of acceleration. The bottom figure displays the percent vertebral body compression during the onset of acceleration.

Analysis of the relative vertical displacement for three-vertebra segments in the upper (T12 to L2) and lower (L3 to L5) lumbar spine during the failure test indicated that the burst fracture likely occurred within 35 ms following the onset of acceleration (Fig. 18). If non-fractured vertebral bodies are considered to be rigid, vertical displacement of the L3 to L5 segment would consist primarily of L3-L4 and L4-L5 intervertebral disc

deformations. Total deformation of the T12-L1 and L1-L2 would be similar in order of magnitude. Therefore, the greater vertical displacement in the upper lumbar spine indicates that the L1 burst fracture at most likely occurred during this period. Likewise, analysis of anterior vertebral body height change indicated that the L4 anterior wedge fracture occurred within the first 44 ms following onset of acceleration (Fig. 18). This kinematic analysis has demonstrated that lumbar spine injuries sustained in the current experimental model occurred during the initial acceleration rise, which corresponded to the time that the experimental acceleration pulse matched the real-world ejection pulse.

4.2.2 Burst Fracture Mechanism

Understanding the specific mechanism is the first step in developing strategies for injury prevention. Although the exact mechanism of burst fractures remains ambiguous to this day, characteristics of the fracture pattern have been observed by several investigators in both clinical and experimental settings. It is characterized by failure of the anterior and middle columns, resulting in a comminuted body, fracture of the posterior wall cortex, and retropulsion of a bone fragment into the spinal canal. In more severe cases the posterior column is injured and there is an increase in interpedicular distance. The current model produced similar results. The injury itself is of utmost importance in the acute and chronic stages because of potential neurological deficit.

Classification of the injury has been a source of much attention in the literature for this reason. Accurate and implementable classification schemes are important to identify clinical instability, which has been defined as the inability of the spine under

physiological loads to maintain relationships between vertebrae so that there is neither initial nor subsequent neurologic deficit, no major deformity, and no severe pain [11]. Much debate has recently emerged on the usefulness of current classifications, and no agreement has been reached on a universal scheme. A uniformly accepted classification is ideal to identify and describe an injury as well as assist physicians in management decisions [113]. It is not the purpose of this thesis to discuss classification schemes, however, the following sources are useful to appreciate and understand the necessity for thoracolumbar injury classifications: [114-119]. As stated earlier, the Denis classification scheme was used to classify the thoracolumbar fractures in the current study [29]. Denis emphasizes that the middle column is the key contributing factor to mechanical instability. Thus, if the posterior body wall is disrupted, spinal instability is likely to be an issue.

Holdsworth was the first to hypothesize the mechanism of the burst fracture. Indeed, the description "burst" originated from his review article in *J Bone Joint Surg Am* [120]. Holdsworth stated, "When severe [vertical compression] force is applied to the top of the head or to the buttocks, one or the other vertebral end plate fractures and the nucleus of the disc is forced into the vertebral body which explodes. The body is shattered from within outward resulting in what I have called a 'burst' fracture." His hypothesis was supported by an earlier work by Roaf [121]. Roaf applied slow vertical compression to functional units and observed the response of the disc by inserting radio-opaque dye into the nucleus pulposus. He observed that the end plate bulged with increasing load and eventually cracked, displacing nuclear material into the vertebral body with further compression. Since then, several authors have noted similar results

following the production of burst fractures. Dissection of fractured vertebral preparations revealed that nuclear material was displaced into the vertebral body via endplate fractures [13,21].

Tran et al. investigated the effect of loading rate on burst fracture characteristics using bovine spines. The study delivered similar energy to the specimens using high and low rate loading via drop-weight and MTS techniques. The resulting post injury CT images and measured peak transient canal occlusions were significantly different, again highlighting the lack of usefulness for an energy threshold for injury. The high loading rate group had a mean canal occlusion of 48%, whereas the low loading rate group had a mean canal occlusion of 7% [12]. Thus, the investigators concluded that the high-rate load application would likely involve neurologic injury, whereas the low rate load application would not. Tran et al. also concluded the study agreeing with the internal pressurization theory proposed by Holdsworth, although without supporting data for evidence. The group stated that hydraulic strengthening by pressurization of internal fluid enhances the compressive strength of the vertebral body, making the compression fracture less likely, and at the same time creates hoop tensile stresses that increase the potential for failure by bursting.

Computational modeling has supported this theory as well. The drop-weight technique was equivalently modeled in the computational environment to monitor stress distribution in a T12-L1 functional unit. At its maximum dynamic compression the endplates bulged towards their vertebral bodies. The highest effective stress was located at the central parts of the endplates adjacent to the nucleus and at the base of the pedicles [122]. These results supported an earlier FE analysis of a functional unit subjected to the

same mechanical conditions imparted in the experimental setting using a MTS machine. It is difficult to analyze these data, however, as only a functional unit was explored. For example, it is interesting that stresses within the cortical bone were concentrated on the posteroinferior parts of T12, as well as the posterosuperior parts of L1 in the study by Qiu et al. Where would the highest stress concentrations be located for an FE model of T12-L5 or T10-L3? Only a validated model of the entire thoracolumbar spine is capable of answering this question.

In clinical burst fractures, the upper posterior region of the vertebral body is the region most often cited as the origin of the retropulsed bony fragments [104,123]. A retrospective clinical study revealed that the cortex of the vertebral canal thinned abruptly at the posterior cortex of the vertebral body at the pedicle height, creating what may be a site for high stress concentration [124]. Experimentally, Hongo et al. recorded surface strain distribution on the middle vertebra (T10, L1, L4) of three-vertebra specimens and reported that fracture initiation during compression loading occurs at the base of the pedicle [24]. The tensile (in the horizontal direction) and compressive (in the vertical direction) strain was also highest in the superior rim compared to the inferior rim in the lumbar region. This was not the case for the thoracic vertebrae tested. What's more, cutting the pedicles resulted in a significant reduction in tensile strain at the base of the pedicle. This led Langrana et al. to hypothesize that anterior shear forces transmitted by the facet joints are responsible for causing the severe canal compromise associated with acute thoracolumbar burst fractures [23]. Langrana et al. tested three-vertebra thoracolumbar specimens in neutral orientation, 15^{o} extension orientation, and in neutral orientation again with the posterior elements removed. The group observed that the

facet joints transmit loads of sufficient magnitude and that specimens tested in 15^{o} extension produced fracture patterns characteristic of acute burst fractures, including an increase in interpedicular distance. However, past studies loading specimens in flexion, an orientation in which the facets are unloaded, produced fracture patterns with severe canal compromise (Table 1). Also, the current study produced canal compromise originating from the upper posterior region of the vertebral body, the most common site, with the specimen in flexion. Thus, data exists to suggest that the facet joints are not critical in determining the degree of injury.

There is also empirical evidence against the theory of an internal bursting mechanism [125]. Ochia and Ching recorded internal pressure measurements during burst fracture formation in human thoracolumbar specimens. The internal pressure changes were measured during 10 mm/s and 2500 mm/s displacement rates. The study revealed that initial peak internal pressure actually decreased from slow- to high-speed tests. The researchers attributed the finding to the associated decrease in strain at failure for high-speed tests, and asserted that vertebral fracture with less displacement would relieve any internal pressure early in the injury event reducing the likelihood that a large internal pressure could occur during or contribute to burst fractures. Thus, internal pressurization may not be a mechanism of injury either. There is inadequate evidence to confidently confirm or refute the theory at the present time.

As stated earlier, burst fractures tend to occur in younger population. Willen et al. noted that vertebrae from subjects above seventy years of age tended to collapse totally in compression due to dynamic axial loading, whereas vertebrae from subjects under forty years of age showed the comminuted fracture pattern characteristic of burst fractures

[13]. Shirado et al. also reported that no burst fractures occurred in specimens with low bone mineral density [21], a typical characteristic of elderly population. These observations may help explain the pathomechanism of burst fracture.

The mechanical function of vertebral bone is partly explained by its composition and architecture. The intrinsic properties of the vertebra's tissue and the arrangement of this tissue allow bone to function effectively under imposed loads, providing strength and resistance to fracture. Bone's composition is made up of fibrous Type I collagen and enmeshed calcium phosphate minerals in a form similar to hydroxypatite [126]. These two chief structural materials provide the inevitable trade-off between toughness and stiffness [127]. The basic vertebra consists of a cortical shell and a trabecular inner core matrix (cancellous bone). During compressive loading, its inner trabecular structure helps dissipate deformation energy without propagation of any formed cracks.

A marked difference in the mechanical response of bone is due to the amount of mineralization. Minerals possess brittle properties, whereas collagen fibrils possess compliant and elastic properties. In osteoporotic vertebrae there is a deficiency in minerals, such as calcium and phosphate. Thus, the bone lacks material that has brittle properties, and the body will have a propensity to collapse under compression loading instead of resulting in a comminuted (brittle-like) fracture. The experimental investigations by Willen et al. and Shirado et al. support this assertion.

What's more, analysis of stress-strain curves obtained from bone in compression has revealed that there is a ductile-to-brittle transition in the type of deformation from low to high strain rates [128-130] . Previous studies have shown that high loading rates, as might be experienced during falls and high speed impacts, lead to increased brittleness

and higher yield strength and stiffness [131-133] . Robertson and Smith in 1978 found the fracture mode of porcine mandibular and bovine femoral bone to be a strong function of strain rate. For both specimens, there was a critical strain rate in which the type of deformation transitioned from ductile- to brittle-like. In addition, recent data suggest an apparent soft-tissue stiffening/strengthening during high-rate loading [101]. Therefore, the entire lumbar spine, i.e., vertebrae and discs, exhibit more stiff and brittle properties with higher loading rates.

Thus, the behavior of the burst fracture may in part be explained by a ductile to brittle transition of bone from lower to higher strain rates. There may be a critical strain rate specific to the lumbar spine in which the vertebrae transitions in a similar fashion. It is important to note, however, that human bone has some post-failure load integrity ("failure" is at the point where the material strength is defined) and therefore cannot be grossly characterized as a brittle material. Nonetheless, to describe the manner in which burst fractures occur as brittle-like is informative, and may be reasonable for identifying the catastrophic nature of the injury.

The exact injury mechanism of burst fractures remains ambiguous. The current experimental model is ideal to investigate this injury, and further testing is warranted.

4.3 Limitations

The current study monitored the onset and progression of soft-tissue injury by recording the maximum flexion ROM. Panjabi et al. suggested dividing the normal ROM into two motion parameters: the neutral zone (NZ) and the elastic zone (EZ) [134].

NZ is a measure of joint laxity, and is defined as the displacement or rotation under approximately zero load. The EZ is defined as the displacement or rotation from the end of the neutral zone to the position under maximum load. The ROM, then, is the sum of the NZ and EZ (Fig. 19).

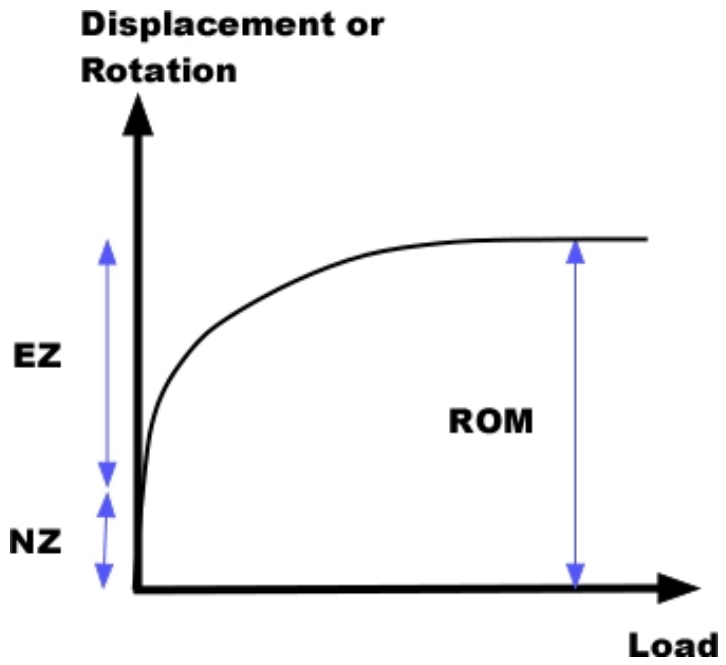

Figure 19: The three motion parameters, EZ, NZ, and ROM, suggested by Panjabi et al. to describe normal spinal kinematics [134].

Oxland and Panjabi compared the sensitivity of the three motion parameters in identifying soft-tissue injury using the drop-weight method and cervical porcine spines. The researchers, using the high-speed weight-drop model, demonstrated that the NZ was the most sensitive motion parameter in defining the onset and progression of spinal (soft-tissue and bony) injury, while the elastic zone parameter did not change significantly with injury. The ROM, consequently, was less sensitive since it was dependent on both the NZ and EZ [135]. However, in a later study using human thoracolumbar specimens, the researchers noted that the NZ and ROM measurements did indeed identify injury at the

same trauma level by both having statistically significant increases. The group confirmed, though, that the NZ was a more sensitive measurement. In the flexion mode, it was found to be 2.3 times more sensitive than the ROM [64]. Thus, the ROM measurements from the flexibility tests in the current study were effective in monitoring spinal injury, but the measurements may have underestimated an injury.

Another possible limitation of this study is the lack of active and passive lumbar musculature in the cadaver model. However, simulated musculature was not incorporated for several reasons. First, simulating physiologic loading in experimental testing is difficult. Although the summed stabilizing forces have been approximated using a follower load in past in vitro testing [136,137], the effect of the preload was shown to have a minor effect on ROM for flexion-extension [138]. Therefore, segmental kinematics obtained in the current study would only be slightly affected. The added complexity was not warranted. Secondly, concerning a computational model, muscle forces are difficult to establish as independent variables [139]. For this reason, it was important to limit the number of parameters during development of the experimental model in light of using the cadaveric data for validation purposes.

CHAPTER 5: CONCLUSIONS

5.1 Implications and Contributions

The present study developed a biomechanically accurate experimental model to investigate lumbar spine injuries during high-rate axial loading. It is the first high-rate axial loading experiment simulating realistic inertial loading with a full-length isolated osteoligamentous lumbar spine, wherein both ends of the specimen were free to move in the vertical direction. This type of loading can be experienced during a military seat ejection from aircraft, underbody blast due to improvised explosive devices, or a fall from height. Acceleration conditions in the current study were biased toward modeling the *boost or in-rail* phase of a military seat ejection sequence. The model is flexible in terms of applied accelerations/loads and location of load application to the superior end of the specimen. Therefore, the model can induce specimen-specific inertial loading via the addition of variable mass to the upper platform, can simulate a wide range of acceleration scenarios by controlling the magnitude, duration, and rate of onset of vertical acceleration, and can model occupants in and out of position (e.g., forward flexed at the time of ejection). Additionally, the wide range of metrics incorporated during model development, including accelerations, loads, segmental kinematics, vertebral body compressions, and pre- and post-test CT images, will permit the identification of accurate injury tolerance thresholds for specific loading scenarios during future testing.

The data obtained herein provide the most comprehensive high-rate response data of the thoracolumbar spine to date. Segmental and overall kinematics were obtained

using realistic boundary conditions. By conducting drop tests with the impacting cylinder at three eccentricities, robust calibration/validation can be done with an FE model of the intact lumbar spine, initiating parametric computational studies investigating injury mitigation.

5.2 Future Research

Little research has been performed to analyze spinal injury systematically under high-speed impact loading conditions [140]. In the past, an arbitrary impact energy was presumably chosen to produce burst fractures. Panjabi systematically established a burst fracture threshold energy using an incremental approach [71]. However, as discussed previously, an energy threshold is inefficient to establish an injury criterion that would be useful in real-world application. The current model is ideal and flexible for studying typical axial loading situations. The injury model was developed to easily control and monitor the parameters of the acceleration and load pulse (magnitude, duration, and rate of onset) and orientation of the spinal column. These parameters have been incorporated in the definition of past injury criterion, and may prove most useful for an axial thoracolumbar injury criterion. Delineating the effects of these factors is also imperative for future safety design considerations not only for ejection seats, but also for the civilian environment. Thus, future testing is warranted to develop an injury criterion for anterior wedge and burst fractures.

Spinal orientation is an important factor in injury patterns since stresses and load distribution among the load bearing tissues is altered. The importance of spinal orientation during seat ejection has been highlighted previously [25,141]. Thus, future

investigations using the developed injury model is warranted to test specimens in different initial orientations to represent in-position and out-of-position. The lumbar spine's orientation during normal upright seating can serve as a basis. Upright sitting with a backrest produces an average of 16.0 ± 8.4 degrees of sacral inclination, defined as the angle between the superior endplate of the S1 vertebra and the horizontal plane parallel to the ground [142]. The total lumbar lordosis (S1-L1) in this orientation is 30.2 ± 13.6 degress.

BIBLIOGRAPHY

[1] F.C. Guill, "Ascertaining the causal factors for 'ejection-associated' injuries," *Aviation, Space, and Environmental Medicine*, vol. 60, 1989, p. B44-B71.

[2] U. Werner, "Ejection associated injuries within the German Air Force from 1981-1997," *Aviation, Space, and Environmental Medicine*, vol. 70, 1999, pp. 1230-1234.

[3] T. Visuri and J. Aho, "Injuries associated with the use of ejection seats in Finnish pilots," *Aviation, Space, and Environmental Medicine*, vol. 63, 1992, pp. 727-730.

[4] W. Sturgeon, *Canadian Forces Aircrew Ejection, Descent, and Landing Injuries*, Downsview, Ontario: 1989.

[5] P. Sandstedt, "Experiences of rocket seat ejections in the Swedish Air Force: 1967-1987," *Aviation, Space, and Environmental Medicine*, vol. 60, 1989, pp. 367-373.

[6] D.G. Newman, "The ejection experience of the Royal Australian Air Force: 1951-92," *Aviation, Space, and Environmental Medicine*, vol. 66, 1995, pp. 45-49.

[7] L. Milanov, "Aircrew Ejections in the Republic of Bulgaria, 1953-93," *Aviation, Space, and Environmental Medicine*, vol. 67, 1996, pp. 364-368.

[8] M.E. Lewis, "Survivability and injuries from use of rocket-assisted ejection seats: analysis of 232 cases," *Aviation, Space, and Environmental Medicine*, vol. 77, 2006, pp. 936-943.

[9] J. Coltman, C. Van Ingen, and F. Selker, *Crash-resistant crewseat limit-load optimization through dynamic testing with cadavers*, Simula, Inc., Phoenix, AZ: 1986.

[10] B.F. Hearon, H.A. Thomas, and J.H. Raddin Jr., "Mechanism of vertebral fracture in the F/FB-111 ejection experience," *Aviation, Space, and Environmental Medicine*, vol. 53, 1982, pp. 440-448.

[11] M.M. Panjabi, T.R. Oxland, M. Kifune, M. Arand, L. Wen, and A. Chen, "Validity of the Three-Column Theory of Thoracolumbar Fractures; A Biomechanic Investigation," *Spine*, vol. 20, 1995, pp. 1122-1127.

[12] N.T. Tran, N.A. Watson, A.F. Tencer, R.P. Ching, and P.A. Anderson, "Mechanism of the Burst Fracture in the Thoracolumbar Spine; The Effect of Loading Rate," *Spine*, vol. 20, 1995, pp. 1984-1988.

[13] J. Willen, S. Lindahl, L. Irstam, B. Aldman, and A. Nordwall, “The Thoracolumbar Crush Fracture; An Experimental Study on Instant Axial Dynamic Loading: The Resulting Fracture Type and Its Stability,” *Spine*, vol. 9, 1984, pp. 624-631.

[14] J.E. Cain, J.T. DeJong, A.S. Dinenberg, R.M. Stefko, C. Platenburg, and W.C. Lauerman, “Pathomechanical analysis of thoracolumbar burst fracture reduction; A calf spine model,” *Spine*, vol. 18, 1993, pp. 1647-1654.

[15] P.C. Cotterill, J.P. Kostuik, J.A. Wilson, G.R. Fernie, and B.E. Maki, “Production of a Reproducible Spinal Burst Fracture for Use in Biomechanical Testing,” *Journal of Orthopaedic Research*, vol. 5, 1987, pp. 462-465.

[16] B.E. Fredrickson, W.T. Edwards, W. Rauschning, J.C. Bayley, and H.A. Yuan, “Vertebral Burst Fractures: An Experimental, Morphologic, and Radiographic Study,” *Spine*, vol. 17, 1992, pp. 1012-1021.

[17] R.K. Wilcox, T.O. Boerger, D.J. Allen, D.C. Barton, D. Limb, R.A. Dickson, and R.M. Hall, “A Dynamic Study of Thoracolumbar Burst Fractures,” *The Journal of Bone & Joint Surgery*, vol. 85A, 2003, pp. 2184-2189.

[18] S.M. Duma, A.R. Kemper, D.M. McNeely, P.G. Brolinson, and F. Matsuoka, “Biomechanical response of the lumbar spine in dynamic compression,” *Biomedical Sciences Instrumentation*, 2006, pp. 476-481.

[19] T. Hoshikawa, Y. Tanaka, S. Kokubun, W.W. Lu, K.D.K. Luk, and J.C.Y. Leong, “Flexion – Distraction Injuries in the Thoracolumbar Spine: An In Vitro Study of the Relation Between Flexion Angle and the Motion Axis of Fracture,” *Journal of Spinal Disorders*, vol. 15, 2002, pp. 139-143.

[20] R.S. Ochia, A.F. Tencer, and R.P. Ching, “Effect of loading rate on endplate and vertebral body strength in human lumbar vertebrae,” *Journal of Biomechanics*, vol. 36, 2003, pp. 1875-1881.

[21] O. Shirado, K. Kaneda, S. Tadano, H. Ishikawa, P.C. McAfee, and K.E. Warden, “Influence of Disc Degeneration on Mechanism of Thoracolumbar Burst Fractures,” *Spine*, vol. 17, 1992, pp. 286-292.

[22] N. Yoganandan, S.J. Larson, F. Pintar, D.J. Maiman, J. Reinartz, and A.J. Sances, “Biomechanics of Lumbar Pedicle Screw/Plate Fixation in Trauma,” *Neurosurgery*, vol. 27, 1990, pp. 873-881.

[23] N.A. Langrana, R.D. Harten, D.C. Lin, M.F. Reiter, and C.K. Lee, “Acute Thoracolumbar Burst Fractures; A New View of Loading Mechanisms,” *Spine*, vol. 27, 2002, pp. 498-508.

[24] M. Hongo, E. Abe, Y. Shimada, H. Murai, N. Ishikawa, and K. Sato, "Surface Strain Distribution on Thoracic and Lumbar Vertebrae Under Axial Compression," *Spine*, vol. 24, 1999, pp. 1197-1202.

[25] C.L. Ewing and A.I. King, "Structural considerations of the human vertebral column under +Gz impact acceleration," *Journal of Aircraft*, vol. 9, 1972, pp. 84-90.

[26] R. Auffret and R.P. Delahaye, *Spinal Injury After Ejection*, Washington, D.C. 20546: 1974.

[27] D.C. Reid, R. Hu, L.A. Davis, and L.A. Saboe, "The Nonoperative Treatment of Burst Fractures of Thoracolumbar Junction," *The Journal of Trauma*, vol. 28, 1988, pp. 1188-1194.

[28] P.C. Mcafee, H.A. Yuan, B.E. Fredrickson, and J.P. Lubicky, "The value of computed tomography in thoracolumbar fractures. An analysis of one hundred consecutive cases and a new classification," *The Journal of Bone & Joint Surgery*, vol. 65, 1983, pp. 461-473.

[29] F. Denis, "The Three Column Spine and its Significance in the Classification of Acute Thoracolumbar Spinal Injuries," *Spine*, vol. 8, 1983, pp. 817-831.

[30] M. Bernhardt and K.H. Bridwell, "Segmental Analysis of the Sagittal Plane Alignment of the Normal Thoracic and Lumbar Spines and Thoracolumbar Junction," *Spine*, vol. 14, 1989, pp. 717-721.

[31] Y. Masharawi, B. Rothschild, G. Dar, S. Peleg, D. Robinson, E. Been, and I. Hershkovitz, "Facet Orientation in the Thoracolumbar Spine; Three-dimensional Anatomic and Biomechanical Analysis," *Spine*, vol. 29, 2004, pp. 1755-1763.

[32] R.J. Kowalski, L.A. Ferrara, and E.C. Benzel, "Biomechanics of the Spine," *Neurosurg Q*, vol. 15, 2005, pp. 42-59.

[33] A.A. White III and M.M. Panjabi, *Clinical Biomechanics of the Spine*, J. B. Lippincott Company, 1978.

[34] R. Watkins, R. Watkins, L. Williams, S. Ahlbrand, R. Garcia, A. Karamanian, L. Sharp, C. Vo, and T. Hedman, "Stability provided by the sternum and rib cage in the thoracic spine," *Spine*, vol. 30, Jun. 2005, pp. 1283-6.

[35] T. Hansson, B. Roos, and A. Nachemson, "The Bone Mineral Content and Ultimate Compressive Strength of Lumbar Vertebrae," *Spine*, vol. 5, 1980, pp. 46-55.

[36] N. Taneja, “Spinal Disabilities in Military and Civil Aviators,” *Spine*, vol. 33, 2008, pp. 2749-2753.

[37] C.P.J. Belmont, C.K.F. Taylor, C.K.T. Mason, C.S.B. Shawen, L.D.W. Polly, and L.W.R. Klemme, “Incidence, Epidemiology, and Occupational Outcomes of Thoracolumbar Fractures among U.S. Army Aviators,” *The Journal of Trauma*, vol. 50, 1997, pp. 855-861.

[38] L. Kazarian and G.A. Graves, “Compressive Strength Charcteristics of the Human Vertebral Centrum,” *Spine*, vol. 2, 1977, pp. 1-14.

[39] J.M. Buckley, L. Cheng, K. Loo, C. Slyfield, and Z. Xu, “Quantitative Computed Tomography-Based Predictions of Vertebral Strength in Anterior Bending,” *Spine*, vol. 32, 2007, pp. 1019 -1027.

[40] R.J. Mcbroom, W.C. Hayes, W.T. Edwards, R.P. Goldberg, and A.A. White, “Prediction of vertebral body compressive fracture using quantitative computed tomography,” *The Journal of Bone & Joint Surgery*, vol. 67, 1985, pp. 1206-1214.

[41] P. Brinckmann, M. Biggemann, and D. Hilweg, “Prediction of the Compressive Strength of Human Lumbar Vertebrae,” *Spine*, vol. 14, 1989, pp. 606-10.

[42] K. Singer, S. Edmondston, R. Day, P. Breidahl, and R. Price, “Prediction of Thoracic and Lumbar Vertebral Body Compressive Strength: Correlations with Bone Mineral Density and Vertebral Region,” *Bone*, vol. 17, 1995, pp. 167-174.

[43] N. Yoganandan, G. Ray, F.A. Pintar, J. Myklebust, and A. Sances Jr, “Stiffness and strain energy criteria to evaluate the threshold of injury to an intervertebral joint,” *Journal of Biomechanics*, vol. 22, 1989, pp. 135-142.

[44] W.C. Hutton and M.A. Adams, “Can the lumbar spine be crushed in heavy lifting?,” *Spine*, vol. 7, 1982, pp. 586-590.

[45] M.A. Adams, W.C. Hutton, and J.R.R. Stott, “The resistance to flexion of the lumbar intervertebral joint,” *Spine*, vol. 5, 1980, pp. 245-253.

[46] M.A. Adams, T.P. Green, and P. Dolan, “The strength in anterior bending of lumbar intervertebral discs.,” *Spine*, vol. 19, Oct. 1994, pp. 2197-203.

[47] S.K. Eswaran, A. Gupta, and T.M. Keaveny, “Locations of bone tissue at high risk of initial failure during compressive loading of the human vertebral body,” *Bone*, vol. 41, 2007, pp. 733 - 739.

[48] Y. Hou and Z. Luo, “A Study on the Structural Properties of the Lumbar Endplate; Histological Structure, the Effect of Bone Density, and Spinal Level,” *Spine*, vol. 34, 2009, pp. 427-433.

[49] A.D. Holmes, D.W.L. Hukins, and A.J. Freemont, “End-plate displacement during compression of lumbar vertebra-disc-vertebra segments and the mechanism of failure,” *Spine*, vol. 18, 1993, pp. 128-135.

[50] V.R. Yingling, J.P. Callaghan, and S.M. Mcgill, “Dynamic loading affects the mechanical properties and failure site of porcine spines,” *Clinical Biomechanics*, vol. 12, 1997, pp. 301-305.

[51] D.T. Watts, E.S. Mendelson, and J.R. Poppen, “Laboratory Test of Aviator□s Ejection Seat,” *Science*, vol. 105, 1947, pp. 583-585.

[52] W.H. Ames, H.M. Sweeney, and H.G. Savely, “Human tolerance to acceleration in pilot ejection,” *Journal of Aviation Medicine*, vol. 18, 1947, pp. 548-553.

[53] J.H. Henzel, G.C. Mohr, and H.E. von Gierke, “Reappraisal of Biodynamic Implications of Human Ejections,” *Aerospace Medicine*, vol. 39, 1968, pp. 231-240.

[54] B.F. Hearon and J.W. Brinkley, “Effect of seat cushions on human response to +Gz impact,” *Aviation, space, and environmental medicine*, vol. 57, 1986, pp. 113-121.

[55] C. Hirsch and A. Nachemson, “New Observations on the Mechanical Behavior of Lumbar Discs,” *1Acta Orthopaedica Scandinavica*, vol. 23, 1954, pp. 184-231.

[56] O. Perey, “Fracture of the vertebral end-plate in the lumbar spine; an experimental biomechanical investigation,” *Acta orthopaedica Scandinavica Supplementum*, vol. 25, 1957, pp. 1-101.

[57] L.-yang Dai, W.-fang Yao, Y.-min Cui, and Q. Zhou, “Thoracolumbar Fractures in Patients with Multiple Injuries: Diagnosis and Treatment — A Review of 147 Cases,” *The Journal of Trauma*, vol. 56, 2004, pp. 348-355.

[58] R.H. Wittenberg, S. Hargus, R. Steffen, G. Muhr, and U. Botel, “Noncontiguous Unstable Spine Fractures,” *Spine*, vol. 27, 2002, pp. 254-257.

[59] C.K. Demetropoulos, K.H. Yang, M.J. Grimm, K.K. Artham, and A.I. King, “High Rate Mechanical Properties of the Hybrid III and Cadaveric Lumbar Spines in Flexion and Extension,” *43rd Stapp Car Crash Conference San Diego, CA, October 25-27, 1999*, 1999.

[60] N. Yoganandan, F.A. Pintar, A. Sances Jr., D.J. Maiman, J.B. Myklebust, G. Harris, and G. Ray, “Biomechanical Investigations of the Human Thoracolumbar Spine,” *SAE Technical Paper Series; 881331*, 1988.

[61] F. Latham, “A study in body ballistics: seat ejection,” *Proceedings of the Royal Society of London*, vol. 147, 1957, pp. 121-139.

[62] K.H. Cooper and F.M.C. Holmstrom, “Injuries during ejection seat training,” *Aerospace Medicine*, vol. 34, 1963, pp. 139-141.

[63] J.L. Hess and C.F. Lombard, “Theoretical investigations of dynamic response of man to high vertical accelerations,” *Journal of Aviation Medicine*, vol. 29, 1958, pp. 66-75.

[64] M.M. Panjabi, M. Kifune, W. Liu, M. Arand, A. Vasavada, and T.R. Oxland, “Graded thoracolumbar spinal injuries: development of multidirectional instability,” *European Spine Journal*, vol. 7, 1998, pp. 332-339.

[65] M.M. Panjabi, M. Kifune, L. Wen, M. Arand, T.R. Oxland, R.-M. Lin, W.-S.S. Yoon, and A. Vasavada, “Dynamic Canal Encroachment During Thoracolumbar Burst Fractures,” *Journal Of Spinal Disorders*, vol. 8, 1995, pp. 39-48.

[66] A.P. Vulcan, A.I. King, and G.S. Nakamura, “Effects of bending on the vertebral column during +Gz acceleration,” *Aerospace Medicine*, vol. 41, 1970, pp. 294-300.

[67] A.I. King, P. Prasad, and C.L. Ewing, “Mechanism of spinal injury due to caudocephalad acceleration,” *Orthopedic Clinics of North America*, vol. 6, 1975, pp. 19-31.

[68] N. Yoganandan, F. Pintar, A.J. Sances, G. Harris, K. Chintapalli, J. Myklebust, D. Schmaltz, J. Reinartz, J. Kalbfleisch, and S. Larson, “Steering wheel induced facial trauma,” *Stapp Car Crash Conference*, Atlanta, GA: 1988, pp. 45-69.

[69] I.A.F. Stokes, “Axis for Dynamic Measurement of Flexion and Extension Torques About the Lumbar Spine; A Computer Simulation,” *Physical Therapy*, vol. 67, 1987, pp. 1230-1233.

[70] S.G. Storvik, N. Yoganandan, F.A. Pintar, and B.D. Stemper, “Experimental induction of lumbar spine compression-flexion injuries,” *Proceedings of the ASME Summer Bioengineering Conference*, June 16-19, Naples, FL: 2010, pp. 1-2.

[71] M.M. Panjabi, H. Ho, Y. Kato, and J. Cholewicki, “Superiority of incremental trauma approach in experimental burst fracture studies,” *Clinical Biomechanics*, vol. 15, 2000, pp. 73-78.

[72] O.K. Atlas, S.D. Dodds, and M.M. Panjabi, “Single and incremental trauma models: a biomechanical assessment of spinal instability,” *European Spine Journal*, vol. 12, 2003, pp. 205-210.

[73] X.-yang Wang, L.-yang Dai, H.-Z. Xu, and Y.-L. Chi, “A comparison of single and incremental impact approaches for producing experimental thoracolumbar burst fractures,” *Journal of Neurosurgery Spine*, vol. 7, 2007, pp. 199-204.

[74] M. Damavandi, N. Farahpour, and P. Allard, “Determination of body segment masses and centers of mass using a force plate method in individuals of different morphology,” *Medical Engineering & Physics*, vol. 31, Nov. 2009, pp. 1187-94.

[75] D.J. Pearsall, J. Gavin Reid, and L.A. Livingston, “Segmental Inertial Parameters of the Human Trunk as Determined from Computed Tomography,” *Annals of Biomedical Engineering*, vol. 24, 1996, pp. 198-210.

[76] N. Yoganandan, F.A. Pintar, J. Zhang, and J.L. Baisden, “Physical properties of the human head: mass, center of gravity and moment of inertia,” *Journal of Biomechanics*, vol. 42, Jun. 2009, pp. 1177-92.

[77] A. Baranto, L. Ekstrom, M. Hellstrom, O. Lundin, S. Holm, and L. Sward, “Fracture Patterns of the Adolescent Porcine Spine: An Experimental Loading Study in Bending-Compression,” *Spine*, vol. 30, 2004, pp. 75- 82.

[78] I. Busscher, A.J.V.D. Veen, J.H.V. Diee, I. Kingma, G.J. Verkerke, and A.G. Veldhuizen, “In Vitro Biomechanical Characteristics of the Spine; A Comparison Between Human and Porcine Spinal Segments,” *Spine*, vol. 35, 2010, pp. 35-42.

[79] M.M. Panjabi, T.R. Oxland, I. Yamamoto, and J.J. Crisco, “Mechanical behavior of the human lumbar and lumbosacral spine as shown by three-dimensional load-displacement curves,” *The Journal of Bone & Joint Surgery*, vol. 76, 1994, pp. 413-424.

[80] Y. Guan, N. Yoganandan, J. Moore, F.A. Pintar, J. Zhang, D.J. Maiman, and P. Laud, “Moment – rotation responses of the human lumbosacral spinal column,” *Journal of Biomechanics*, vol. 40, 2007, pp. 1975-1980.

[81] “Essentials of Motion Capture (version 4.5),” *Vicon Motion Systems*, 2002, pp. 1-62.

[82] Society Of Automotive Engineers (SAE), *Instrumentation for impact test - Part 1 - Electronic instrumentation*, Warrendale, PA: .

[83] D.E. Harrison, D.D. Harrison, R. Cailliet, S.J. Troyanovich, T.J. Janik, and B. Holland, “Cobb Method or Harrison Posterior Tangent Method; Which to Choose for Lateral Cervical Radiographic Analysis,” *Spine*, vol. 25, 2000, pp. 2072-2078.

[84] D.E. Harrison, D.D. Harrison, R. Cailliet, T.J. Janik, and B. Holland, “Radiographic Analysis of Lumbar Lordosis; Centroid, Cobb, TRALL, and Harrison Posterior Tangent Methods,” *Spine*, vol. 26, 2001, pp. 235-242.

[85] R.W. Nightingale, J.H. Mcelhaney, W.J. Richardson, and B.S. Myers, “Dynamic responses of the head and cervical spine to axial impact loading,” *Journal of Biomechanics*, vol. 29, 1996, pp. 307-318.

[86] M.M. Panjabi, T.R. Oxland, R.-M. Lin, and T.W. McGowen, “Thoracolumbar Burst Fracture; A Biomechanical Investigation of Its Multidirectional flexibility,” *Spine*, vol. 19, 1994, pp. 578-585.

[87] R.W. Nightingale, D.L. Camacho, A.J. Armstrong, J.J. Robinette, and B.S. Myers, “Inertial properties and loading rates affect buckling modes and injury mechanisms in the cervical spine,” *Journal of Biomechanics*, vol. 33, 2000, pp. 191-197.

[88] J.P. Dickey and D.J. Kerr, “Effect of specimen length: are the mechanics of individual motion segments comparable in functional spinal units and multisegment specimens?,” *Medical Engineering & Physics*, vol. 25, 2003, pp. 221-227.

[89] M. Bernstein, “Easily missed thoracolumbar spine fractures,” *European Journal of Radiology*, vol. 74, 2010, pp. 6-15.

[90] L.E. Mermelstein, R.F. McLain, and S.A. Yerby, “Reinforcement of Thoracolumbar Burst Fractures With Calcium Phosphate Cement: A Biomechanical Study,” *Spine*, vol. 23, 1998, pp. 664-670.

[91] C.C. Ward and G.K. Nagendra, “Mathematical Models: Animal and Human Models,” *The Biomechanics of Trauma*, A.M. Nahum and J. Melvin, eds., Norwalk, CT: Appleton-Century-Crofts, 1985, pp. 77-100.

[92] C.T. Terry and V.L. Roberts, “A VISCOELASTIC MODEL OF THE HUMAN SUBJECTED TO + gz ACCELERATIONS,” *Journal of Biomechanics*, vol. 1, 1968, pp. 161-168.

[93] J.W. Brinkley and J.T. Shaffer, *Dynamic Simulation Techniques for the design of escape systems: Current applications and future air force requirements*, Ohio: 1971.

[94] D. Orne and Y.K. Liu, “A mathematical model of spinal response to impact,” *Journal of Biomechanics*, vol. 4, 1971, pp. 49-71.

[95] P. Prasad, A.I. King, and C.L. Ewing, “The role of articular facets during +Gz acceleration,” *Journal of Applied Mechanics, Transactions of the ASME*, vol. 41, 1974, pp. 321-326.

[96] P. Prasad and A.I. King, “An Experimentally Validated Dynamic Model of the Spine,” *Journal of Applied Mechanics, Transactions of the ASME*, vol. 41, 1974, pp. 546-550.

[97] B.D. Stemper, N. Yoganandan, and F. a Pintar, “Validation of a head-neck computer model for whiplash simulation,” *Medical & biological engineering & computing*, vol. 42, May. 2004, pp. 333-8.

[98] Y. Guan, N. Yoganandan, J. Zhang, F. a Pintar, J.F. Cusick, C.E. Wolfla, and D.J. Maiman, “Validation of a clinical finite element model of the human lumbosacral spine.,” *Medical & biological engineering & computing*, vol. 44, Aug. 2006, pp. 633-41.

[99] M.A. Adams and W.C. Hutton, “The Mechanical Function of the Lumbar Apophyseal Joints,” *Spine*, vol. 8, 1983, pp. 327-330.

[100] P. Brinckmann, W. Frobin, E. Heirholzer, and M. Horst, “Deformation of the Vertebral End-plate Under Axial Loading of the Spine,” *Spine*, vol. 8, 1983, pp. 851-856.

[101] S.H.M. Brown, D.E. Gregory, and S.M. McGill, “Vertebral end-plate fractures as a result of high rate pressure loading in the nucleus of the young adult porcine spine,” *Journal of Biomechanics*, vol. 41, 2008, pp. 122-127.

[102] J.L. Gunning, J.P. Callaghan, and S.M. Mcgill, “Spinal posture and prior loading history modulate compressive strength and type of failure in the spine: a biomechanical study using a porcine cervical spine model,” *Clinical Biomechanics*, vol. 16, 2001, pp. 471-480.

[103] R.J. Parkinson and J.P. Callaghan, “Clinical Biomechanics The role of dynamic flexion in spine injury is altered by increasing dynamic load magnitude,” *Clinical Biomechanics*, vol. 24, 2009, pp. 148-154.

[104] R.K. Jelsma, P.T. Kirsch, L.F. Jelsma, W.C. Ramsey, and J.F. Rice, “Surgical treatment of thoracolumbar fractures,” *Surgical Neurology*, vol. 18, Sep. 1982, pp. 156-66.

[105] L. Calenoff, J.W. Chessare, L.F. Rogers, J. Toerge, and J.S. Rosen, “Multiple Level Spinal Injuries: Importance of Early Recognition,” *American Journal Roentgenology*, vol. 130, 1978, pp. 665-669.

[106] R.L. Henderson, D.C. Reid, and L.A. Saboe, “Multiple Noncontiguous Spine Fractures,” *Spine*, vol. 16, 1991, pp. 128-131.

[107] F. Denis, G.W.D. Armstrong, K. Searls, and M. L, “Acute Thoracolumbar Burst Fractures in the Absence of Neurologic Deficit; A Comparison Between Operative and Nonoperative Treatment,” *Clinical Orthopaedics and Related Research*, vol. 189, 1984, pp. 142-149.

[108] B.T. Ragel, C.D. Allred, S. Brevard, R.T. Davis, and E.H. Frank, "Fractures of the Thoracolumbar Spine Sustained by Soldiers in Vehicles Attacked by Improvised Explosive Devices," *Spine*, vol. 34, 2009, pp. 2400 -2405.

[109] D.F. Shanahan and M.O. Shanahan, "Injury in U.S. Army Helicopter Crashes October 1979-September 1985," *Journal of Trauma*, vol. 29, 1989, pp. 415-423.

[110] D. Richter, M.I. Hahn, P.A.W. Ostermann, A. Ekkernkamp, and G. Muhr, "Vertical deceleration injuries : a comparative of the injury patterns of 101 patients after accidental and intentional high falls," *Injury*, vol. 27, 1996, pp. 655-659.

[111] J.M. Hsu, T. Joseph, and A.M. Ellis, "Thoracolumbar fracture in blunt trauma patients: guidelines for diagnosis and imaging," *Injury*, vol. 34, 2003, pp. 426-433.

[112] J. Inamasu and B.H. Guiot, "Thoracolumbar junction injuries after motor vehicle collision: are there differences in restrained and nonrestrained front seat occupants?," *Journal of Neurosugery Spine*, vol. 7, 2007, pp. 311-314.

[113] M.K. Sethi, A.J. Schoenfeld, C.M. Bono, and M.B. Harris, "The evolution of thoracolumbar injury classification systems," *The Spine Journal*, vol. 9, 2009, pp. 780-788.

[114] C.M. Bono, A.R. Vaccaro, R.J. Hurlbert, P. Arnold, F.C. Oner, J. Harrop, and N. Anand, "Validating a Newly Proposed Classification System for Thoracolumbar Spine Trauma: Looking to the Future of the Thoracolumbar Injury Classification and Severity Score," *Injury*, vol. 20, 2006, pp. 567-572.

[115] A.A. Patel, A. Dailey, D.S. Brodke, M. Daubs, J. Harrop, P.G. Whang, and A.R. Vaccaro, "Thoracolumbar spine trauma classification: the Thoracolumbar Injury Classification and Severity Score system and case examples," *Journal of Neurosurgery Spine*, vol. 10, 2009, pp. 201-206.

[116] P.M. Tsou, J. Wang, L. Khoo, A.N. Shamie, and L. Holly, "A thoracic and lumbar spine injury severity classification based on neurologic function grade, spinal canal deformity, and spinal biomechanical stability," *Spine*, vol. 6, 2006, pp. 636-647.

[117] A.R. Vaccaro, E.M. Baron, J. Sanfilippo, S. Jacoby, J. Steuve, E. Grossman, M. Dipaola, P. Ranier, L. Austin, R. Ropiak, M. Ciminello, C. Okafor, M. Eichenbaum, V. Rapuri, E. Smith, F. Orozco, P. Ugolini, M. Fletcher, J. Minnich, G. Goldberg, J. Wilsey, J.Y. Lee, M.R. Lim, A. Burns, R. Marino, C. Dipaola, L. Zeiller, S.C. Zeiler, J. Harrop, D.G. Anderson, T.J. Albert, and A.S. Hilibrand, "Reliability of a Novel Classification System for Thoracolumbar Injuries: The Thoracolumbar Injury Severity Score," *Spine*, vol. 31, 2006, pp. 62-69.

[118] P.G. Whang, A.R. Vaccaro, K.A. Poelstra, A.A. Patel, D.G. Anderson, T.J. Albert, A.S. Hilibrand, J.S. Harrop, A.D. Sharan, J.K. Ratliff, R.J. Hurlbert, P. Anderson,

B. Aarabi, L.H.S. Sekhon, R. Gahr, and J.A. Carrino, “The Influence of Fracture Mechanism and Morphology on the Reliability and Validity of Two Novel Thoracolumbar Injury Classification Systems,” *Spine*, vol. 32, 2007, pp. 791-795.

[119] L.-yang Dai, S.-dan Jiang, X.-yang Wang, and L.-sheng Jiang, “A review of the management of thoracolumbar burst fractures,” *Surgical Neurology*, vol. 67, 2007, pp. 221 - 231.

[120] S.F. Holdsworth, “Review Article; Fractures, Dislocations, and Fracture-Dislocations of the Spine Spine,” *The Journal of Bone & Joint Surgery*, vol. 52, 1970, pp. 1534-1551.

[121] R. Roaf, “A study of the mechanics of spinal injuries,” *The Journal of Bone & Joint Surgery*, vol. 42B, 1960, pp. 810-823.

[122] T.-xia Qiu, K.-wee Tan, V.-sin Lee, and E.-chon Teo, “Investigation of thoracolumbar T12 – L1 burst fracture mechanism using finite element method,” *Medical Engineering & Physics*, vol. 28, 2006, pp. 656-664.

[123] R.K. Jelsma, P.T. Kirsch, J.F. Rice, and L.F. Jelsma, “The radiographic description of thoracolumbar fractures,” *Surgical Neurology*, vol. 18, Oct. 1982, pp. 230-6.

[124] M.H. Heggeness and B.J. Doherty, “The trabecular anatomy of thoracolumbar vertebrae: implications for burst fractures,” *Journal of Anatomy*, vol. 191 (Pt. 2, Aug. 1997, pp. 309-12.

[125] R.S. Ochia and R.P. Ching, “Internal Pressure Measurements During Burst Facture Formation in Human Lumbar Vertebrae,” *Spine*, vol. 27, 2002, pp. 1160-1167.

[126] D.B. Burr, “The Contribution of the Organic Matrix to Bone’s Material Properties,” *Bone*, vol. 31, 2002, pp. 8 -11.

[127] J.D. Currey, “Mechanical Properties of Bone Tissues with Greatly Differing Functions,” *Journal of Biomechanics*, vol. 12, 1979, pp. 313-319.

[128] J.H. McElhaney, “Dynamic response of bone and muscle tissue,” *Journal of Applied Physiology*, vol. 21, Nov. 1966, pp. 1231-1236.

[129] D.M. Robertson and D.C. Smith, “Compressive Strength of Mandibular Bone as a Function of Microstructure and Strain Rate,” *Journal of Biomechanics*, vol. 11, 1978, pp. 455-471.

[130] R.R. Adharapurapu, F. Jiang, and K.S. Vecchio, “Dynamic fracture of bovine bone,” *Materials Science & Engineering*, vol. 26, 2006, pp. 1325 - 1332.

[131] R.M. Kulin, F. Jiang, and K.S. Vecchio, “Loading rate effects on the R-curve behavior of cortical bone,” *Acta biomaterialia*, vol. 7, Sep. 2010, pp. 724-32.

[132] L.J. Gibson, “The mechanical behaviour of cancellous bone,” *Journal of Biomechanics*, vol. 18, 1985, pp. 317-328.

[133] U. Hansen, P. Zioupos, R. Simpson, J.D. Currey, and D. Hynd, “The effect of strain rate on the mechanical properties of human cortical bone,” *Journal of Biomechanical Engineering*, vol. 130, Mar. 2008, pp. 1-8.

[134] M.M. Panjabi, “Biomechanical Evaluation of Spinal Fixation Devices: I. A Conceptual Framework,” *Spine*, vol. 13, 1988, pp. 1129-1134.

[135] T.R. Oxland and M.M. Panjabi, “The onset and progression of spinal injury: A demonstration of neutral zone sensitivity,” *Journal of Biomechanics*, vol. 25, 1992, pp. 1165-1172.

[136] A.G. Patwardhan, R.M. Havey, K.P. Meade, B. Lee, and B. Dunlap, “A follower load increases the load-carrying capacity of the lumbar spine in compression,” *Spine*, vol. 24, 1999, pp. 1003-1009.

[137] A.G. Patwardhan, R.M. Havey, A.J. Ghanayem, H. Diener, K.P. Meade, B. Dunlap, and S.D. Hodges, “Load-carrying capacity of the human cervical spine in compression is increased under a follower load,” *Spine*, vol. 25, 2000, pp. 1548-1554.

[138] A. Rohlmann, S. Neller, L. Claes, G. Bergmann, and H.-joachim Wilke, “Influence of a Follower Load on Intradiscal Pressure and Intersegmental Rotation of the Lumbar Spine,” *Spine*, vol. 26, 2001, pp. 557-561.

[139] V.K. Goel and L.G. Gilbertson, “Applications of the finite element method to thoracolumbar spinal research - past, present, and future,” *Spine*, vol. 20, 1995, pp. 1719-1727.

[140] C.K. Lee, Y.E. Kim, C.S. Lee, Y.M. Hong, J.M. Jung, and V.K. Goel, “Impact response of the intervertebral disc in a finite-element model,” *Spine*, vol. 25, Oct. 2000, pp. 2431-9.

[141] Y.K. Liu and U.R. Pontius, *THE EFFECTS OF INITIAL SPINAL CONFIGURATION ON PILOT EJECTION; USAARL REPORT NO. 74-6*, Fort Rucker, Alabama: 1973.

[142] F. Lin, S. Parthasarathy, S.J. Taylor, D. Pucci, R.W. Hendrix, and M. Makhsous, “Effect of Different Sitting Postures on Lung Capacity, Expiratory Flow, and Lumbar Lordosis,” *Archives of Physical Medicine and Rehabilitation*, vol. 87, 2006, pp. 504-509.

Appendix A

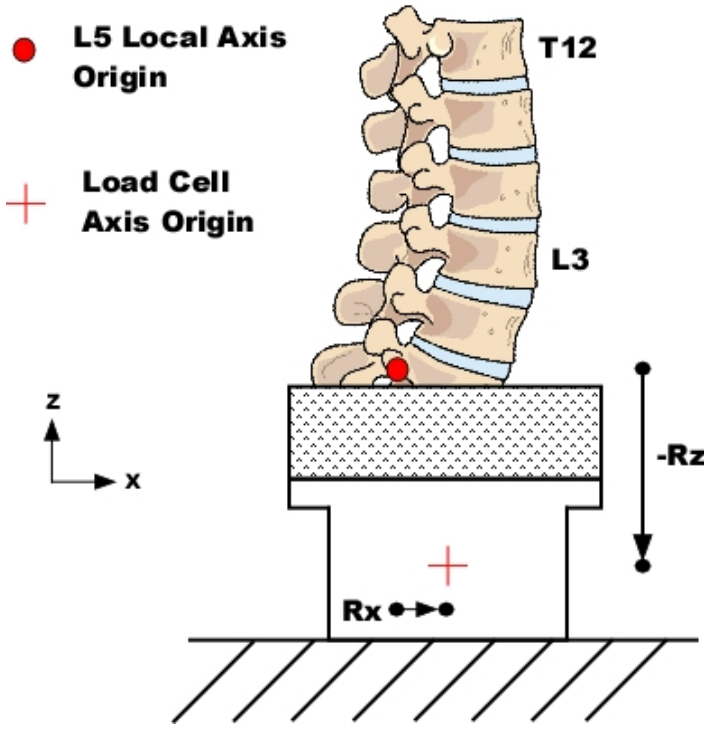

Figure 20: Illustration describing transferred load data. Axis definitions follow the right hand rule. Rz and Rx is the distance measured between the two origins.

The loads recorded by the six-axis load cell were transferred to the local axis origin of L5 according to the equations below. The sign from Rz and Rx were carried from the axes definitions illustrated in Fig. 20.

$$Fx_{L5} = Fx_{LC}$$
$$Fy_{L5} = Fy_{LC}$$
$$Fz_{L5} = Fz_{LC}$$
$$Mx_{L5} = Mx_{LC} - Rz * Fy_{LC}$$
$$My_{L5} = My_{LC} + Rz * Fx_{LC} - Rx * Fz_{LC}$$
$$Mz_{L5} = Mz_{LC} + Rx * Fy_{LC}$$